

1 **Palaeoenvironment reconstruction, volcanic evolution and geochronology of the Cerro Blanco**  
2 **subcomplex, Nevados de Chillán Volcanic Complex, central Chile.**

3 <sup>1\*</sup> Katy Mee, <sup>1</sup> Jennie S. Gilbert, <sup>2</sup> David W. McGarvie, <sup>3</sup> José A. Naranjo, and <sup>4</sup> Malcolm S. Pringle.

4  
5 <sup>1</sup> Lancaster Environment Centre, Faculty of Science and Technology, Lancaster University, Lancaster, LA1  
6 4YQ, UK

7 <sup>2</sup> Department of Earth Science and Environmental Sciences, The Open University, Walton Hall, Milton  
8 Keynes, MK7 6AA, UK

9 <sup>3</sup> Servicio Nacional de Geología y Minería, Avenida Santa María 0104, Providencia, Santiago, Chile, e-mail:  
10 jnaranjo@sernageomin.cl

11 <sup>4</sup> Department of Earth, Atmospheric and Planetary Sciences, 77 Massachusetts Avenue, Massachusetts Institute  
12 of Technology, Cambridge, MA, 02139-4307, USA

13 \* Now at: British Geological Survey, Keyworth, Nottingham, UK, NG12 5GG, Tel: + 44 (0)115 936 3100, Fax:  
14 +44 (0)115 936 3200, E-mail: katy@bgs.ac.uk

15  
16 **Abstract**

17 Nevados de Chillán Volcanic Complex, central Chile, has been active for at least 640 ka – a period spanning a  
18 number of glacial and interglacial periods. Geologic mapping, radiometric dating and geochemical analysis  
19 have identified six new volcanic units and produced five new <sup>40</sup>Ar/<sup>39</sup>Ar ages for Cerro Blanco, the northern  
20 subcomplex of Nevados de Chillán volcano. Compositions range from dacite to basaltic-andesite and a new  
21 geologic map is presented.

22 Examination of lava fracture structures on both newly mapped lavas and those mapped during previous  
23 studies has enabled interpretations of former eruptive environments. Palaeoenvironment reconstructions,  
24 combined with <sup>40</sup>Ar/<sup>39</sup>Ar ages and comparison with the marine oxygen isotope record, show that at least three  
25 phases of volcanic activity have occurred during the evolution of Cerro Blanco: (1) a constructive, pre-caldera  
26 collapse period; (2) a period of caldera formation and collapse; and (3) a constructive period of dome growth  
27 forming the modern day volcanic centre. This style of volcanic evolution, whereby large-scale caldera collapse  
28 is followed by growth of a new stratocone is common at Andean volcanoes.

29  
30 **Keywords:** *volcano-ice interaction, Nevados de Chillán, Cerro Blanco, palaeoenvironment reconstruction,*  
31 *snow-contact, caldera-collapse, <sup>40</sup>Ar/<sup>39</sup>Ar dating*

32

33

### Introduction

34 Nevados de Chillán Volcanic Complex (NCVC) is situated at 36°S, 71°W in the Southern Volcanic Zone  
35 (SVZ) of the Andean cordillera, central Chile. It is a large stratovolcano composed of two volcanic centres  
36 situated 6 km apart along a NNW-SSE trending axis (Fig. 1) (Dixon et al., 1999).

37 The two subcomplexes of Nevados de Chillán, Cerro Blanco and Las Termas, lie at the NW and SE  
38 ends of the axis, respectively (Fig. 2). The Las Termas subcomplex is predominantly dacitic, whilst Cerro  
39 Blanco is predominantly basaltic-andesite to andesite in composition (Dixon et al., 1999). Volcanic products  
40 include subaerial, subglacial and snow-contact lavas, pyroclastic flow deposits, tephra, lahar deposits and  
41 scoria cones (Dixon et al., 1999; Mee et al., 2006). High precision  $^{40}\text{Ar}/^{39}\text{Ar}$  and  $^{14}\text{C}$  analysis reveals that the  
42 volcano has been active since at least 640 ka, with the eruption of the subglacial Los Pincheira lavas, which  
43 have an estimated remaining volume of 10 km<sup>3</sup> (Dixon et al., 1999). Activity continues to the present day, with  
44 recent eruptions occurring during September 2003 from the Las Termas subcomplex (Naranjo and Lara, 2004)  
45 and then in January 2009 (<http://www.volcanolive.com/chillan.html>).

46 Cerro Blanco is composed of several volcanic cones, each with their associated lavas. The most recent  
47 of these lavas, the Santa Gertrudis scoria cone and lava, was erupted between 1861 and 1865 (Dixon et al.,  
48 1999; Mee et al., 2006) and dominates the northwestern flank of Cerro Blanco. To the north and west of Cerro  
49 Blanco are curved cliff sections interpreted by Déreulle and Déreulle (1974) as remnants of two caldera walls  
50 (Fig. 1). Although this theory is now generally accepted, evidence is restricted to the morphological structure  
51 of the cliff scarps, clearly visible in the field and on aerial photographs. The inner cliff sections are thought to  
52 represent a younger caldera approximately 5 km in diameter, with the outer cliffs suggesting an older caldera of  
53 approximately 10 km in diameter (Fig. 1).

54 Geologic mapping by Dixon et al. in 1999 concentrated on the cone and flanks of the Cerro Blanco  
55 and Las Termas subcomplexes and the surrounding valleys, with volcanic products being assigned to the  
56 appropriate subcomplex on the basis of geochemistry. The highly complex caldera wall areas were thus  
57 grouped together as CB1 (the Lanahue Lavas of Dixon et al., 1999), covering an area of ~ 15 km<sup>2</sup>. Since much  
58 of the area is dominated by steep-sided and scree covered slopes, interpretation of stratigraphic relationships are  
59 mostly confined to the caldera wall cliffs, hence field mapping for this project was concentrated in these  
60 localities. Detailed mapping during 12 weeks of fieldwork in 2001 and 2002, have allowed us to identify three  
61 new volcanic units along the outer caldera wall (OCW) and upper Santa Gertrudis valley and three new  
62 volcanic units along the inner caldera wall (ICW) and these are presented in a new geologic map (Fig. 3).

63 Volcanic facies from each of these units are described in two sections: (1) the outer caldera wall and upper  
64 Santa Gertrudis valley (SGV) units and facies, and (2) the inner caldera wall units and facies.

65 We interpret the palaeoenvironment of emplacement of each of these facies. These interpretations are  
66 combined with geochemical data,  $^{40}\text{Ar}/^{39}\text{Ar}$  dates and evidence from the marine oxygen isotope record (MOIR)  
67 to evaluate the volcanic evolution of Cerro Blanco. It must be noted that accessibility to most of the exposed  
68 rock around the outer caldera wall and Santa Gertrudis valley is severely limited due to the extreme topography,  
69 and although access can be gained via the foot of the Santa Gertrudis valley to the north, this was beyond the  
70 scope of this project. Geochemical and radiometric analyses are therefore limited for these units but  
71 observations are included for completeness.

72

### 73 **Field observations and petrography**

74 Field observations for each of the newly mapped units are described below. Table 1 summarises the field  
75 observations and Table 2 gives a summary of the geochemistry and petrology for each newly mapped unit.  
76 Further geochemical data are provided with the online version of this article. The distributions of newly  
77 mapped and existing units at Cerro Blanco are provided in Figure 3.

78

#### 79 **1. Santa Gertrudis valley and the outer caldera wall**

80 The upper reaches of the Santa Gertrudis valley (SGV) begin ~ 2.5 km to the north of the Cerro Blanco summit,  
81 where several tributaries collect runoff from the north and western flanks of Cerro Blanco, the ICW and the  
82 OCW before deflecting north into the Río Santa Gertrudis and the Santa Gertrudis valley proper. From Cerro  
83 Blanco, only the tops of the cliffs can be accessed. Here, the valley is ~ 30 m wide with near vertical cliff faces  
84 of 100-200 m in height. The north and south sides of the valley appear to be comprised of two entirely different  
85 lithologic units (SGV1 and SGV2, respectively), with the outer caldera wall unit (OC1) making up the third  
86 newly mapped unit in this locality.

87

#### 88 **SGV1 – North Santa Gertrudis valley lava**

89 Despite earlier mapping by Dixon et al. (1999) identifying the lavas in this area as the 81.5 ka old CB1  
90 Lanalhue Lavas, it is clear from the much greater degree of weathering and alteration, that the lava on the north  
91 side of the Santa Gertrudis valley is much older and must be considered as a separate unit (SGV1). The SGV1  
92 lava exhibits a mixture of chaotic, hackly joints and irregular columnar joints. The latter are ~ 10-20 cm in  
93 width and sometimes up to 1 m in length, although are generally much less than this. Since the cliff face was

94 inaccessible, detailed measurements of column orientation and geometry was not possible. The lava itself is  
95 dark orange-brown and heavily weathered in appearance and geochemical analysis reveals this unit to be  
96 andesitic in composition (69 wt % SiO<sub>2</sub>) (Table 2).

97

### 98 **SGV2 – South Santa Gertrudis valley sequence**

99 The SGV2 unit on the south side of the valley is, by contrast, much more complex with four separate facies  
100 identified (Fig. 4). It is likely that each of these facies represents a separate geologic unit but since detailed  
101 studies of the cliffs were prevented by poor accessibility the facies have been grouped together for simplicity.  
102 The base of the cliffs is comprised of ~ 100 m thickness of massive, slightly weathered lava with no obvious  
103 fracture patterns or bedding (Zone 1). Above this, lies a 10-70 m thick section of pale grey, fine-grained and  
104 bedded material (Zone 2). This becomes thinner towards the west where it comes into contact with a 40 m  
105 thick lens of columnar jointed lava (Zone 3). The succession is complete by the IC2 lava lobes (discussed later),  
106 which is the only part of the cliff face that can be accessed from the cliff tops and hence no samples of the  
107 SGV2 unit could be collected for geochemical or radiometric analysis.

108

### 109 **OC1 – Outer caldera wall lavas and breccias**

110 Overlying the SGV1 lava on the north side of the valley is the outer caldera wall (Fig. 1). It is ~ 2.5 km long  
111 and comprises at least 10 separate, andesite (60 wt % SiO<sub>2</sub>) lavas flow deposits, each 5-10 m thick and inter-  
112 bedded with irregular layers (< 3 m thick) of red scoriaceous material (Fig. 5). Towards the western end of the  
113 OCW where the upper elevation is ~ 50 m lower than the eastern end, the lava is extremely polished and  
114 exhibits two sets of striae with variable orientations. The first set of striae is broad and deep and has the same  
115 weathered surfaces of the surrounding rocks. The second set, which cuts through the first, is much sharper and  
116 narrower, with fresher grey surfaces. On both the west and east sides of the Santa Gertrudis valley, small  
117 patches of breccia are banked up against the OC1 lavas. The east side of the valley was inaccessible but  
118 observations through binoculars reveal that the breccia is bedded, dips gently (< 10°) to the south and contacts  
119 unconformably with the adjacent OC1 lava.

120

### 121 **2. Inner caldera wall units and facies**

122 The inner caldera wall (ICW) is also ~ 2.5 km long and curves around the northwestern flank of Cerro Blanco  
123 (Figs. 1 and 3). It is characterised by a topographic high at each end: Lanalhue at the southern extremity and  
124 the North Ridge at the northern extremity (Fig. 1). Three different volcanic units have been identified along the

125 ICW, each with characteristic facies: the inner caldera wall lavas (IC1), the inner caldera wall vent facies (IC2)  
126 and a series of lava lobes, sills and dykes (IC3).

127

### 128 **IC1 – Inner caldera wall lavas**

129 The inner caldera wall lavas are best exposed at the southern end of the ICW, where at least six individual lava  
130 flow deposits can be observed in the south-facing cliffs (Figs. 6 and 7). The near vertical caldera wall scarp  
131 cuts through the IC1 lavas to the east and a 25 m wide band of the lava is exposed half-way up the cliff face,  
132 with scree obscuring the lower 20-30 m and the IC2 Lanalhue vent topping the sequence (Fig. 6). Each layer is  
133 3-8 m thick and extends westwards (away from Cerro Blanco) for 10-100 m. Whilst the two upper and two  
134 lower lava flows dip gently westwards ( $\sim 5^\circ$ ), the two central lavas are much less uniform and in places the lava  
135 has draped over the underlying lavas forming several bulbous and hackly jointed lobes (Fig. 7). The two upper  
136 and two lower lavas exhibit broad columnar jointing and scoriaceous upper margins, whilst the two central  
137 lavas are bulbous in places, with glassy texture and hackly or pseudopillow fractures (Mee et al., 2006).  
138 Individual lava flows are separated by irregular patches of breccia, which is comprised of 5-40 cm angular  
139 clasts of lava in a pale grey and fine-grained matrix. The geochemical composition of the lava flows range  
140 from basaltic-andesite (54 SiO<sub>2</sub> wt %) to dacite (65 SiO<sub>2</sub> wt %).

141

### 142 **IC2 – Inner caldera wall vent facies**

143 The topographic highpoints at either end of the ICW (Lanalhue and the North Ridge) are characterised by  
144 remnants of volcanic vents. At the southern Lanalhue end, a 50 m thick cross-section through the vent facies is  
145 exposed towards the top of the inner caldera wall cliffs (Fig. 8). Several facies can be identified at the Lanalhue  
146 and North Ridge vent locations, ranging in composition from basaltic andesite (55 wt % SiO<sub>2</sub>) to andesite (59  
147 wt % SiO<sub>2</sub>). The main constituent, present at both localities, is a series of bedded and welded breccia and  
148 spatter deposits. Secondly is a vesicular, andesitic body, which is exposed in the Lanalhue vent cross-section at  
149 the southern end of the inner caldera wall. Thirdly, is the Upper Santa Gertrudis valley (USGV) lava, which  
150 first crops out on the eastern flanks of the North Ridge and is exposed eastwards to the top of the Santa  
151 Gertrudis valley. These facies are described in more detail below and in Tables 1 and 2, with the exception of  
152 the USGV lava, which is the subject of a more detailed study by Mee et al. (2006) and hence is only  
153 summarised here.

154

155 *Welded breccia and spatter*

156 A cross-section through the Lanalhue vent exposes an ~ 20 m thick sequence of andesitic, bedded breccia and  
157 spatter, displaying varying degrees of welding. Figure 9 summarises the typical structure and composition of  
158 the vent. The beds can be traced southwards for up to 70 m, where they form a fanned array with the thickness  
159 of the beds increasing from 25 cm to 3 m with distance from the centre of the vent. The dip of the beds  
160 increases upwards through the succession from near horizontal to 45° S (i.e. back towards the centre of the  
161 vent). The structure of each bed becomes more chaotic towards the centre of the vent and, in places, exhibits  
162 substantial brecciation, slumping and faulting (Fig. 9). Contacts between the beds are often unconformable,  
163 particularly close to the centre of the vent. Clast-supported, polymict breccia containing angular to heavily  
164 smeared glassy lithics and scoria bombs, fills the centre of the vent (Fig. 9). A grey, platy dyke from the IC3  
165 unit (described below) cuts through this breccia at an angle of ~ 85° S. Small, 2-3 cm clasts of the dyke have  
166 been incorporated into the adjacent breccia (Fig. 9).

167 To the north, any beds that were deposited are now obscured by a 50 m wide and up to 15 m high  
168 andesitic body. The texture is massive and vesicular with no bedding or fracturing. Vesicles are roughly  
169 spherical and range in size from 0.1-2 cm, with large vesicle accumulations of > 45 cm in diameter also present.  
170 The contact between the andesite body and the surrounding breccia is gradational over ~ 30 cm, with clasts of  
171 breccia being incorporated into the andesite.

172 To the north, the highest point along the ICW reaches 2456 m at the top of the North Ridge. Here, a  
173 small plateau of ~ 0.5 km<sup>2</sup> that slopes gently to the NW (away from the summit of Cerro Blanco) also exhibits a  
174 series of welded breccia and spatter beds (Fig. 10). The beds form a curved, semi-circular array at the southern  
175 end of the North Ridge (nearest to the Cerro Blanco summit) and exhibit similar features and structures as the  
176 welded breccia and spatter beds of the Lanalhue vent (Fig. 9). As the North Ridge slopes away from Cerro  
177 Blanco, dropping in elevation from 2456 m to 2375 m, the vent facies become increasingly polished and eroded  
178 and is marked by one set of striations.

179

#### 180 *Upper Santa Gertrudis valley (USGV) lava*

181 The andesitic, USGV lava can be divided into three textural and geomorphological zones, each occurring at  
182 different elevations (Table 1): autobrecciated and elongate lava lobes with pseudopillow fractures at the upper  
183 elevations; interconnected, hackly-jointed lava lobes and hyaloclastite at the mid-elevations; and glassy,  
184 columnar-jointed lava at the lower elevations. Detailed descriptions and palaeoenvironment interpretations for  
185 these facies and the Santa Gertrudis lava are given in Mee et al. (2006).

186

187 **ICW3 – Subglacial lobes, sills and dykes**

188 This unit can be divided into two facies: (1) a series of grey platy sills and dykes cutting through the inner  
189 caldera wall vent sequence and in places cropping out onto the current topographic surface; and (2) glassy lava  
190 lobes situated on the col to the south of the Lanalhue vent sequence (Fig. 6) and on the north and eastern flanks  
191 of the North Ridge (Fig. 10).

192

193 *Platy sills and dyke*

194 The sills and dykes are 1-3 m thick, with narrow (> 1-2cm) platy fractures aligned parallel to the flow surfaces.  
195 Several platy sills cut below the IC2 andesite intrusion and in places have breached the ground surface on and  
196 above the col to the north of the Lanalhue sequence (Fig. 8). In one case, a sill has breached the ground surface  
197 at an elevation of ~2375 m in the col region to the north of the Lanalhue vent (Fig. 11). The lava can be  
198 followed laterally for less than 2 m before being reduced to scree and has a 10-15 cm thick, red scoriaceous  
199 upper surface (Fig. 11). The scree is estimated to cover an area of at least 100 m<sup>2</sup>.

200 A 2 m wide dyke also cuts through the IC1 cliffs and is exposed on the volcano-facing scarp (Fig. 8).  
201 It appears to feed a small laccolith at its top, which is exposed below the southern end of the IC2 welded  
202 breccia and spatter beds. Poor accessibility meant that detailed observations of this structure were limited.  
203 However, a sample collected by Dixon et al. (1999) during their 1996 expedition, is now known to have come  
204 from base of this dyke (Jennie Gilbert, oral communication 2006).

205

206 *Glassy lava lobes*

207 Several bulbous and glassy lava lobes crop out on the col that separates the Lanalhue ridge from the central  
208 regions of the ICW and on the north and eastern flanks of the North Ridge. The best examples of these lobes  
209 are two steep-sided lava lobes on the col to the north of the Lanalhue vent (Figs. 6 and 11). The more easterly  
210 of the two lobes is 7 m high and 14 m wide, whilst the more westerly of the two lobes is 12 m high and 8 m  
211 wide. Both are bulbous in shape and have steep (> 45° to near vertical) outer margins, particularly those facing  
212 down-slope. In between these two larger lobes are several smaller (~ 1 m diameter), interconnected lobes (Fig.  
213 11). The outer margins of the lobes are 25-50 cm thick and dominated by narrow (8-15 cm in diameter with 4-8  
214 sides), glassy hackly joints. The interior of the lobes is, by contrast, holocrystalline with 10-30 cm thick  
215 concentric fractures that break around phenocrysts. Irregular patches of yellow, clast-supported and unbedded  
216 breccia is observed at the bases of the two larger lobes and surrounding the smaller lobes in the scree (Figure  
217 11). In places, finger-like structures of the breccia curve upwards into the overlying lava lobe (Fig. 11).

218

219

#### <sup>40</sup>Ar/<sup>39</sup>Ar analysis

220 By determining the ages of volcanic units that have been interpreted as having erupted under certain conditions  
221 (e.g. subglacially, in contact with snow/ice or subaerially), we are able to: (1) confirm their stratigraphic  
222 position at Cerro Blanco and, (2) compare ages with the record of global temperature (marine oxygen isotope  
223 record) in order to confirm that the interpreted conditions would have been likely at the time of eruption.  
224 Alternatively, if field observations suggest that a lava was cooled under a substantial thickness of ice, yet  
225 radiometric dates suggest that the volcano should not have been covered by snow or ice at the time of eruption,  
226 then this would trigger further study of either the volcanic fracture patterns and stratigraphic relationships or  
227 radiometric dates to ensure that the most confident interpretations were reached.

228

#### 229 **Sample selection**

230 After establishing stratigraphic relationships in the field, eight samples were selected for <sup>40</sup>Ar/<sup>39</sup>Ar analysis. All  
231 of these samples came from the inner caldera wall units, since poor accessibility to the outer caldera wall and  
232 Santa Gertrudis valley made it impossible to obtain samples suitable for dating. Samples were chosen on the  
233 basis of:

- 234 1. Palaeoclimatic importance – a mixture of subaerial, subglacial and snow-contact lavas were chosen to  
235 enable correlation of the inferred eruptive environment with the marine oxygen isotope record. It was  
236 anticipated that the ages of these samples would span a glacial/interglacial transition.
- 237 2. Stratigraphic importance – i.e. those units that displayed key stratigraphic relationships with other  
238 units not chosen for analysis; and
- 239 3. Compositional/petrographic suitability for <sup>40</sup>Ar/<sup>39</sup>Ar dating – thin sections of all samples were studied  
240 to select samples with the least amount of chemical alteration or other possible sources of  
241 contamination.

242 Following petrographic analysis, it was obvious that many of the more glassy rocks (and therefore those most  
243 likely to have erupted during subglacial conditions) would be unsuitable for <sup>40</sup>Ar/<sup>39</sup>Ar analysis and hence fewer  
244 of these units were analysed than was originally intended. Whole rock and groundmass separates were  
245 analysed at the Scottish Universities Research and Reactor Centre (SURRC), East Kilbride, Scotland, using the  
246 same <sup>40</sup>Ar/<sup>39</sup>Ar incremental-heating procedures as Dixon et al., (1999), which are more fully described in Singer  
247 and Pringle (1996) and Harford et al., (2002). To deem these dates acceptable, the following criteria were used  
248 (Pringle, 1993; Singer and Pringle, 1996):

- 249 1. At least 3 contiguous high-temperature steps representing 50 % of the  $^{39}\text{Ar}$  must be used in the age  
250 calculation.
- 251 2. These steps must be below the F-variate critical value (Pringle, 1993; Taylor, 1982; Harford et al.,  
252 2002; York, 1969).
- 253 3. The plateau and isochron ages (Pringle, 1993; Singer and Pringle, 1996) must be concordant with one  
254 another (i.e. their errors should overlap).
- 255 4. The isochron  $^{40}\text{Ar}/^{36}\text{Ar}$  intercept should not be significantly different from the atmospheric argon value  
256 of 295.

257

## 258 **Results**

259 In total, 8 samples from Cerro Blanco were selected for analysis, each representing different volcanic facies.  
260 Two samples (from IC1 and OC1) did not produce a full data set to enable age calculations and two others  
261 (from IC1 and IC3) produced high errors and should, at best, be considered reconnaissance age estimates. The  
262 remaining four samples have yielded acceptable ages, although they represent only two of the newly mapped  
263 units (IC2 and IC3). Table 3 gives a full summary of both the new and published (Dixon et al., 1999)  $^{40}\text{Ar}/^{39}\text{Ar}$   
264 analyses for Cerro Blanco and the complete data repository is available from the journal's electronic archive.

265 The IC2 unit has yielded three acceptable ages:  $92.4 \pm 3.5$  ka for the andesite intrusion located to the  
266 north of the Lanalhue vent;  $90.0 \pm 0.6$  ka for the upper Santa Gertrudis Valley lava; and  $88.9 \pm 1.0$  ka for the  
267 welded breccia and spatter beds of the North Ridge. A sample of the IC3 lava lobes, sills and dykes has  
268 produced two acceptable ages from different splits of the same sample. Specifically, this sample comes from  
269 the sill that has breached the ground surface above the col region at the southern end of the ICW. This unit has  
270 been dated at  $80.0 \pm 0.6$  ka and  $79.9 \pm 0.6$  ka.

271

272

## 272 **Discussion**

273 In recent years Cerro Blanco has had a permanent icecap and an even larger distribution of seasonal snow (Fig.  
274 2). Fracture structures associated with snow and/or ice contact appear to be common features of the volcanic  
275 units on Cerro Blanco. The distribution and extent of these fractures is vital for interpretation of the local  
276 climatic conditions at the time of eruption.

277 The following sections use field observations and stratigraphic relationships to help interpret the  
278 eruptive settings of volcanic units at Cerro Blanco, particularly in terms of the presence or absence of snow and  
279 ice at the time of eruption. We consider the various phases of volcanic evolution of Cerro Blanco and draw

280 comparisons with other Andean volcanoes. Finally, where  $^{40}\text{Ar}/^{39}\text{Ar}$  analysis has been successful, the ages are  
281 compared with the marine oxygen isotope record (MOIR) to confirm that field and stratigraphic observations of  
282 each unit are concordant with climatic conditions at the time of eruption, i.e. if a lava is interpreted as having  
283 erupted under a large thickness of ice, this should be supported by global ice volumes according to the MOIR.

284

### 285 *Palaeoenvironment interpretations*

#### 286 *The Santa Gertrudis valley and outer caldera wall*

287 At depths of nearly 200 m, the Santa Gertrudis valley is likely to have been an important runoff channel for  
288 several hundred thousands of years. The presence of narrow, hackly and chaotic columnar joints on the SGV1  
289 lavas on the north side of the valley supports the presence of water during their emplacement, although the lack  
290 of pillow structures suggests that this was not entirely subaqueous. The chaotic nature of the columns is  
291 therefore interpreted as the upper, entablature zone of a two-tiered lava flow (Degraff et al., 1989). This is  
292 similar in structure to the upper zone of the Los Pincheira lavas (Dixon et al., 1999), which was interpreted by  
293 Dixon et al. to have cooled against glacial ice with meltwater causing the fine-scale penetrative jointing of the  
294 entablature zone (Lescinsky and Sisson, 1998). Whether the entablature zone of the SGV1 lava was caused by  
295 glacial meltwater or runoff from the volcano is unclear since the lower portions of the cliffs were inaccessible.

296 The outer caldera wall cliffs, which lie stratigraphically above the SGV1 lavas, have been interpreted  
297 by Déreulle and Déreulle (1974) as remnants of an ancient caldera wall on account of the abrupt cliff faces  
298 separating the recent volcanic cones at the centre of the complex from the older, shallow-dipping lavas to the  
299 west and north. The broad, columnar joints, holocrystalline texture and scoriaceous upper surfaces of the lava  
300 flows are indicative of slow cooling and hence the OC1 lavas are inferred to be subaerial (Cas and Wright,  
301 1987). Deep glacial striae and polishing to the upper surfaces of the cliffs at the western end of the OCW,  
302 suggest that the cliffs have been subjected to repeated glaciations. By contrast, the eastern end of the OCW,  
303 where elevation is 50-100 m higher, does not exhibit the same degree of polishing, suggesting that snow, ice  
304 and water in this area were diverted into the Santa Gertrudis valley.

305 The complex mixture of facies on the south side of the Santa Gertrudis valley (SGV2) are clearly not  
306 part of the SGV1 or OC1 units on the north side of the valley. Since detailed observations of the cliffs could  
307 not be made, it is not possible to make meaningful interpretations of the different facies that make up SGV2. It  
308 is possible, however, to make inferences about relative ages of the units despite the lack of  $^{40}\text{Ar}/^{39}\text{Ar}$  ages, since  
309 the high levels of weathering to the north side of the valley (SGV1 and OC1), suggest they are much older than

310 the SGV2 unit on the south side of the valley. This adds further support to the interpretation of OC1 as caldera  
311 wall cliffs, with the SGV2 unit representing the downthrown side of a caldera wall fault.

312

### 313 *The inner caldera wall*

314 The northern extremity of the inner caldera wall is 'overlapped' by the outer caldera wall cliffs, which form an  
315 amphitheatre around the north and western flanks of the North Ridge. This, along with the presence of two sets  
316 of glacial striae and a greater degree of weathering on the outer caldera wall lavas compared to one set of  
317 glacial striae on the inner caldera wall units, leads us to believe that the inner caldera wall cliffs and their  
318 associated geologic units are younger than those of the outer caldera wall and Santa Gertrudis valley.

319 The IC1 lavas are the most extensive, covering an area of at least 1 km<sup>2</sup>, although it is likely that they  
320 extend up to a further 2 km north, through the central region of the inner caldera wall (Figs. 3 and 4). It is also  
321 likely that the IC1 lavas were, at one time, more extensive to the east but have since been cut by the inner  
322 caldera wall fault with any remnants now obscured by scree and the more recent Colcura cone and lavas (Dixon  
323 et al., 1999).

324 Each layer of the IC1 unit is thought to represent a separate pulse of lava that flowed west away from  
325 the current Cerro Blanco stratocone. The two upper and two lower lava flows, with their crystalline interiors  
326 and scoriaceous tops, exhibit characteristics typical of subaerial lavas (Cas and Wright, 1987). Although the  
327 overall dip of the lavas is west, away from Cerro Blanco, in places the two central lavas appear to have  
328 followed topographic depressions causing the morphology to be bulbous in places (Figs. 5 and 6). Hackly and  
329 pseudopillow fractures on the lava in these locations, along with their glassy texture, suggest that these lobes  
330 were cooled rapidly, either by steam, water or snow (Lescinsky and Fink, 2000; Mee et al., 2006). The lack of  
331 fragmental material (and the local distribution of ice-contact features) indicates that water did not accumulate in  
332 any great volume, hence it is unlikely that a thick ice sheet was present during the time of eruption (Lescinsky  
333 and Fink, 2000; Lescinsky and Sisson, 1998). Since snow and ice are persistent throughout the year at  
334 elevations of ~ 2300 m and upwards (i.e. the approximate elevation at which the IC1 lavas are exposed) it is  
335 more likely that portions of the lava flowed over or into snow and ice that had accumulated in topographic  
336 depressions, with steam and water from the melting snow causing hackly and pseudopillow fractures.

337 The IC2 vent facies is best exposed at the southern end of the ICW with the cross-section through the  
338 Lanalhue vent. Several beds of welded breccia and spatter represent successive pulses of a small (< 0.25 km<sup>2</sup>)  
339 eruption. The increasing dip of the beds towards the centre of the vent, suggests that material tended to  
340 accumulate at distances of 50-70 m from the vent. The presence of unconformable contacts, brecciation and

341 faulting within the deposits at the mouth of the vent suggests a greater degree of instability with proximity to  
342 the vent. Slumping within the beds has produced rheomorphic structures indicating that material flowed back  
343 towards the vent after initial deposition (Sumner and Branney, 2002). Finally, the small andesitic body was  
344 intruded to the north side of the vent. It is suggested that the breccia that now fills the vent was part of the lava  
345 intrusion and that the high level of oxidation is due to contact with either snow or water during intrusion  
346 (Naranjo et al., 1992). Since the dyke was well insulated from the breccia, its high temperature was preserved,  
347 enabling the formation of the platy, welded and sheared structure during the high-pressure intrusion (Fig. 9).  
348 The final facies associated with the IC2 unit is the Upper Santa Gertrudis valley (USGV) lava, which is exposed  
349 on the eastern flanks of the North Ridge and in the upper reaches of the Santa Gertrudis valley. The gradation  
350 from one textural zone to another has led to the interpretation of a multi-phase cooling history of the lava,  
351 consisting of subaerial, snow-contact and then ice-constraint cooling environments at successively lower  
352 elevations (Mee et al., 2006).

353         The youngest unit associated with the inner caldera wall is IC3, a series of platy sills and dykes and  
354 glassy lava lobes. Where one of the dykes has breached the ground surface, the scoriaceous and vesicular top  
355 suggest it cooled subaerially (Cas and Wright, 1987) yet the glassy texture and polygonal, pseudopillow  
356 fractures on the base are indicative of snow-contact (Mee et al., 2006). Although the preserved lava only  
357 persists for 2 m, the large volume of scree ( $\sim 0.1 \text{ km}^2$ ) suggests that, at one time, the lava was much more  
358 extensive. It is likely that melting snow at the base of the lava combined with the heavily fractured and  
359 extremely brittle lava interior caused the lava to collapse.

360         Several pieces of evidence suggest that the glassy lava lobes, which are exposed at a lower elevation in  
361 the col to the north of the Lanalhue vent, were glacially cooled. Firstly, the glassy and hackly jointed outer  
362 carapaces, which protect the more crystalline interior, imply quenching of the lava and fracture by steam  
363 penetration (Lescinsky and Fink, 2000). Since the lobe interiors are relatively crystalline compared to their  
364 glassy outer carapaces, quenching and solidification of the carapace must have allowed the fluid lava of the  
365 interior to cool more slowly and develop a larger crystal size (Lescinsky and Fink, 2000). Secondly, cooling  
366 fractures can be used to infer the palaeo-cooling surface of a fractured lava body since they form perpendicular  
367 to the cooling surface (Lescinsky and Sisson, 1998). Although the chaotic nature of hackly joints means that  
368 measurement of individual fracture surfaces would be unlikely to give true orientations of any former cooling  
369 surfaces, the presence of the quenched carapaces surrounding the remaining body of lava suggests they were  
370 entirely enveloped by the cooling surface at the time of emplacement.

371           The presence of hyaloclastite breccia around the base of the lobes would suggest that some degree of  
372 interaction with water occurred (Tuffen et al., 2001; Tuffen et al., 2002a, 2002b). However, since there is a  
373 lack of any ash-grade fragmental material (produced by phreatomagmatic activity) it seems unlikely that a large  
374 amount of water was present. In addition to this, there are several factors that suggest that the  
375 palaeotopography was similar to that of today and hence that water would have constantly drained down slope.  
376 Firstly, part of the breccia beneath the more westerly of the two lobes has been folded upwards (Fig. 11c and d)  
377 into the base of the lobe, suggesting that some degree of post-emplacment gravitational slumping occurred.  
378 Secondly, the steep, sub-vertical front surfaces of the lobes suggest that they were constrained down-slope by a  
379 near vertical, robust cooling surface, such as ice (Fig. 11). Finally, the more easterly of the two IC3 lobes  
380 drapes either side of the existing col (Fig. 11a and b), suggesting that a similar topography to that of today was  
381 present during the time of emplacement. All these factors favour down-slope drainage of water away from the  
382 lava lobes, thus making it virtually impossible for significant volumes of water to have accumulated. It is,  
383 therefore, more likely that the surrounding breccia was caused by intrusion of the sills through a waterlogged  
384 substrate (Tuffen et al., 2001; Tuffen et al., 2002a, 2002b) followed by disaggregation and brecciation. Breccia  
385 at the base of the lobes is most likely to have been caused by further quenching and brecciation of the lava as it  
386 slumped downwards.

387           Since the base of one of the sills that breached the ground surface appears to have been cooled by  
388 snow-contact (Mee et al., 2006) rather than subglacially, it may be used in conjunction with the subglacial lava  
389 lobes at a lower elevation on the col to estimate the approximate upper level of ice at the time of emplacement  
390 (Fig. 12). For example, we know that the sill penetrated the ground surface above the Lanalhue col at the  
391 current altitude of ~ 2325 m. The glassy, quenched texture on the base of the lava suggests that it was rapidly  
392 cooled, most likely due to snow-contact given the presence of pseudopillow fractures (Mee et al., 2006). It is  
393 thought that as the ice and snow retreated, any lava that had flowed over the snow and cooled would have  
394 collapsed, resulting in the large volume of scree that remains in the vicinity today. In this case, 2325 m would  
395 have been the approximate upper limit of ice (Fig. 12). Sills lower down in the col region (at ~ 2250 m  
396 elevation) were emplaced subglacially causing constraint of the lava, which enabled quenching and  
397 solidification of the outer carapace and resulted in the steep front surfaces observed on the lobes today. In  
398 addition, the subglacial lobes on the north and eastern flanks of the North Ridge also appear to have been  
399 emplaced subglacially at 2275m, further supporting the inference of the upper level of ice between 2275m and  
400 2325m. Figure 12 shows our interpretation of the palaeoenvironment into which the IC3 sills and lobes were

401 emplaced. From our interpretation we think that a valley glacier was present on Cerro Blanco approximately 80  
402 ka ago and that the IC3 lobes were ice-constrained.

403

#### 404 *Volcanic evolution and caldera formation*

405 Since detailed geochemical analyses have not been conducted during this study, the magmatic evolution of  
406 Cerro Blanco is not discussed and to do so would require further investigation. Instead, we focus on the  
407 chronology of eruptive events at Cerro Blanco and discuss caldera formation.

408 Volcanic units at Cerro Blanco appear to fall into two categories: (1) those that erupted from a central  
409 vent (or vents) producing voluminous (up to 10 km<sup>3</sup>) lava flows that dip and radiate away from the current  
410 volcanic centre; and (2) those which erupted from smaller vents along the caldera wall faults and tend to be  
411 localised and less voluminous (< 1 km<sup>3</sup>). The oldest known units to be associated with Nevados de Chillán  
412 volcano are the Los Pincheira lavas at 640 ka old, which are thought to be part of the early development of the  
413 volcanic complex due to their radial distribution around the volcano before either caldera was formed (Dixon et  
414 al., 1999). The next oldest units are those that make up the Santa Gertrudis valley and caldera wall lavas  
415 (SGV1, SGV2, OC1 and IC1). These all fall into the former category of lavas erupted from a central vent and  
416 we believe these to be part of an older complex for the following reasons:

- 417 1. The lavas all dip away from the caldera wall and therefore appear to have originated from much higher up  
418 the volcano, towards the current summit of Cerro Blanco. Although their exact sources are unknown, they  
419 show no evidence of having erupted along a caldera wall fault.
- 420 2. They are estimated to be at least twice the (preserved) volume of the IC2 and IC3 units, which extend for  
421 only a short distance (20-200 m) away from the caldera wall. By contrast, the inner and outer caldera wall  
422 lavas are 50-150 m in thickness and extend up to 1 km away from the volcano. The Santa Gertrudis valley  
423 sequences are 100-200 m in thickness and occupy the entire Santa Gertrudis valley. All appear to be much  
424 more weathered and altered than the IC2 and IC3 units.

425 The age constraints for this older complex are rather loose (640-90 ka old) but they are dissected by at least two  
426 caldera-forming events. A lack of detailed study of the outer caldera wall makes it impossible to infer the  
427 timing of caldera formation, unlike the inner caldera where ages of both pre- and post-caldera collapse units  
428 provide a relatively tight timescale for caldera formation. The cross-section through the Lanalhue vent at the  
429 southern end of the inner caldera wall is clear evidence that the vent facies (IC2) were emplaced prior to caldera  
430 formation, since the caldera fault cuts through this unit. By contrast, the IC3 unit crops out on the col region to  
431 the south of the Lanalhue vent where it has draped down the caldera wall fault, suggesting that the

432 palaeotopography was similar to present day and hence suggesting IC3 was emplaced post-caldera formation.  
433 This would put the caldera collapse event that produced the inner caldera wall at between 90 and 80 ka BP,  
434 which agrees with the Pleistocene age interpreted by Naranjo et al. (1994) and Dixon et al. (1999).

435 Several volcanic facies have been identified along the inner caldera wall, all of which have been  
436 assigned to the IC2 vent unit. Since three of these ages ( $92.4 \pm 3.5$  ka,  $90.0 \pm 0.6$  ka and  $88.9 \pm 1.0$  ka) are  
437 statistically indistinguishable, the exact order of eruptions at either end of the caldera wall is uncertain, although  
438 they are likely to have been simultaneous. The strong lithological and chronological correlation between the  
439 vent sequences at each end of the inner caldera wall facies suggests that volcanic activity was occurring along  
440 the entire length of the inner caldera wall at ca. 90 ka. It is quite possible that eruption of the IC2 vent facies  
441 created the initial fracture lines along which caldera collapse ultimately occurred, with subsequent eruptions  
442 over the following millennia (i.e. of the IC3 unit) continuing to exploit these structural weaknesses.

443 Some time after eruption along the caldera fault, volcanism switched to the modern Cerro Blanco and  
444 Las Termas subcomplexes with lavas being erupted from several vents located around either stratocone (Dixon  
445 et al., 1999). At the latest, this would have occurred at 23.9 ka ago given the age of the oldest known lava to  
446 have erupted from the modern Cerro Blanco cone (i.e. CB2a of Dixon et al., 1999). This stratocone has been  
447 active as recently as 1865 with the eruption of the Santa Gertrudis lava (Dixon et al., 1999; Mee et al., 2006).

448 The combination of extreme topography and large accumulations of snow and ice make access to all  
449 remnants of the caldera walls (inner and outer) very difficult. Since this project has focussed primarily on the  
450 Cerro Blanco subcomplex it is not possible to make any accurate interpretations of caldera forming  
451 mechanisms, which of course would apply to the entire Nevados de Chillán Volcanic Complex and not just the  
452 Cerro Blanco subcomplex. It is unclear by what mechanism the calderas at Cerro Blanco (and hence Nevados  
453 de Chillán) formed but there are many models that have been applied to Andean volcanoes. Through the  
454 Central Volcanic Zone (CVZ) and the northern sector of the Southern Volcanic Zone (SVZ), caldera collapse is  
455 often attributed to large-magnitude explosive volcanism, characterised by plinian fall deposits and ignimbrites  
456 (Gilbert et al., 1996). Such deposits do occur at Nevados de Chillán, particularly to the south and west of the  
457 Las Termas subcomplex (Dixon et al., 1999), but these have not been studied or mapped in detail and thus it is  
458 unknown whether they are related to any caldera-forming process. By contrast, caldera formation at the  
459 predominantly mafic volcanoes of the southern SVZ, show less evidence to suggest they formed by explosive  
460 volcanism (Gilbert et al., 1996).

461 At Sollipulli, Gilbert et al. (1996) describe how the caldera was filled with a large body of ice (volume  
462  $> 6 \text{ km}^3$ ) soon after caldera collapse and that subsequent volcanic eruptions occurred along the caldera margins

463 rather than under the greatest thickness of ice (i.e. towards the centre of the caldera). This is, at least in part,  
464 similar to the eruption of the IC3 subglacial lobes, dykes and sills along the inner caldera wall after caldera  
465 collapse, and it is certain that the caldera was at least partially filled with ice (up to ~ 2325 m; Fig. 12) during  
466 this time. However, it must be noted that if any volcanism had occurred towards the centre of the caldera, the  
467 modern Cerro Blanco complex would now cover these units.

468 Volcanic units erupted from the Cerro Blanco subcomplex can be assigned to three periods of volcanic  
469 activity: (1) the older, pre-caldera collapse complex; (2) caldera formation and eruption along the inner caldera  
470 wall fault and (3) the modern volcanic complex. This type of evolution whereby caldera collapse is followed  
471 by growth of a new stratocone is common at many Andean volcanoes. At Nevado del Tolima, Colombia,  
472 Thouret et al. (1995) describe four periods of eruptive activity. The early period produced Quaternary age  
473 basement lava flows, followed by the formation of an ancient stratovolcano, which has since been cut by  
474 caldera formation. A second stratovolcano was subsequently formed and is now overlain by the modern Tolima  
475 complex. The early constructive phase of volcanism at Puyehue, Chile, is estimated to comprise 80 % of the  
476 total volume and is characterised by two broad shields (Singer et al., 2008). The modern Puyehue stratovolcano  
477 has since been built on the more southerly of these two shields (Singer et al., 2008). Clavero et al. (2004) have  
478 identified four stages of volcanic evolution at Parinacota volcano, Chile: (1) the early formation of dome  
479 complexes and associated pyroclastic deposits; (2) formation of a steep-sided stratocone on top of this dome  
480 complex; (3) partial collapse of the volcanic edifice; and (4) formation of a new steep-sided stratocone and  
481 several flank cones.

482 At Cerro Blanco, the early, constructive phase of volcanism is characterised by the eruption of  
483 multiple, shallow-dipping lava flows that make up the Santa Gertrudis valley and both the outer and inner  
484 caldera wall units (i.e. SGV1, SGV2, OC1 and IC1). The more localised eruptions along the inner caldera wall,  
485 that produced the vent facies (IC2) and subglacial lava lobes (IC3), coincide with a period of caldera formation  
486 and collapse when volcanism was restricted to the caldera wall fault. Finally, volcanism switched to the centre  
487 of the complex with the production of the modern Cerro Blanco stratocone.

488

#### 489 *Comparison with the marine oxygen isotope record*

490 Figure 13 shows the chronology of eruptions at Cerro Blanco over the past ca. 120 ka, alongside the marine  
491 oxygen isotope record (MOIR) where oxygen isotope variations are used as a proxy for global ice volumes.  
492 The lack of  $^{40}\text{Ar}/^{39}\text{Ar}$  ages for the older Cerro Blanco subcomplex makes it difficult to assign them to a  
493 particular stage of the MOIR and although we know a minimum age of 92.4 ka, they are likely to be much

494 older. Prior to 92.4 ka, early volcanic activity at Cerro Blanco produced the inner and outer caldera wall lavas  
495 (OC1 and IC1), the platform on which the modern volcanic subcomplex is built. A large amount of volcanic  
496 activity occurred between ca. 80-92.4 ka during the second half of marine oxygen isotope stage (MOIS) 5,  
497 when eruptions were apparently confined to the edges of the caldera. The eruption of the IC2 vent facies at ca.  
498 90 ka is thought to coincide with the initial formation of the inner caldera wall fault, and subaerial textures on  
499 the vent facies suggest that, locally at least, ice was lower than 2300 m. By ca. 80 ka, when the IC3 dykes, sills  
500 and subglacial lobes were emplaced, the inner caldera was formed and was likely to have been filled with ice.  
501 The upper level of the ice can be constrained to between 2275 m and 2325 m (the approximate elevation of the  
502 caldera rim) given the presence of subaerial, snow-contact and subglacial features on the same unit (Fig. 12)  
503 (Mee et al., 2006). It is likely that a combination of an ice-filled caldera and the presence of the inner caldera  
504 wall fault caused the eruption of the IC3 unit to be confined to the rim of the caldera (Gilbert et al., 1996).

505 An apparent hiatus in volcanic activity at Cerro Blanco occurred between 80 and 25 ka, although  
506 eruptions were taking place elsewhere on Nevados de Chillán (Dixon et al., 1999). When volcanism returned to  
507 Cerro Blanco, focus had shifted to the centre of the complex with the eruption of the CB2 Colcura and eastern  
508 units, which Dixon et al. (1999) suggest are remnants of a probable post-caldera collapse shield volcano,  
509 overlain by remnants of a steep-sided andesitic stratocone. Ages for this unit suggest it would have been  
510 erupted during the last glacial maxima in the area, which occurred between 33.5-14 ka according to Lowell et  
511 al. (1995). It is unknown, however, if this unit exhibits any subglacial or ice-contact features that would be  
512 consistent with widespread glaciation. Subsequent eruptions at Cerro Blanco, up to and including the eruption  
513 of the Santa Gertrudis (CB4) lava between 1861-1865 (Dixon et al., 1999) have continued to build the modern  
514 stratocone.

515

516

## Conclusions

517

518 1. Identification of volcanic facies characteristic of subaerial, subaqueous, subglacial, ice-constraint and  
519 snow-contact activity is important for establishing past eruptive environments and particularly for  
520 establishing palaeoclimate conditions at the time of an eruption. Ages of glacially-cooled lavas can be  
521 compared with the marine oxygen isotope record to confirm whether or not large amounts of snow and ice  
522 were likely to have been present on the volcano at the time of an eruption. Volcanic facies are, therefore,  
523 powerful tools for palaeoclimate reconstruction as well as for interpreting past eruptive environments.

524

- 525 2. Six new volcanic units, each displaying a wide range of volcanic facies, have been identified along the  
526 inner caldera wall, the outer caldera wall and in the upper Santa Gertrudis valley of Cerro Blanco and a  
527 new geologic map has been produced.  
528
- 529 3. The North and South Santa Gertrudis valley units, and the outer and inner caldera wall units (SGV1,  
530 SGV2, OC1 and IC1, respectively) are thought to represent an older volcanic complex, characterised by  
531 voluminous ( $> 10 \text{ km}^3$ ), constructional volcanism; a feature which is typical of many Andean volcanoes.  
532
- 533 4. The inner caldera wall fault was an important location for volcanism between 100 and 80 ka BP, during  
534 which time it is thought that the inner caldera wall was formed. At ca. 90 ka BP, volcanism was occurring  
535 at both ends of the inner caldera walls producing welded breccia and spatter beds on the ridge tops and  
536 subglacial lavas (USGV lava) in the valleys, suggesting that a small valley glacier was present at the time  
537 of eruption. At ca. 80 ka BP, after the inner caldera wall had been formed, a series of sills and dykes was  
538 intruded along the inner caldera wall, some of which were intruded into ice below a level of  $\sim 2325 \text{ m}$ ,  
539 producing subglacial lobes.  
540
- 541 5. Volcanic evolution at Cerro Blanco can be divided into three periods of eruptive activity: (1) constructive,  
542 pre-caldera collapse volcanism; (2) caldera formation and collapse; and (3) formation of the modern Cerro  
543 Blanco stratocone. This volcanic cycle is typical at many Andean volcanoes.  
544

#### 545 **Acknowledgements**

546 The authors would like to thank Hugh Tuffen and Mike James for their valuable contributions in the field, along  
547 with Holly Frey and Charles Stern for their thorough reviews, all of which have considerably improved this  
548 manuscript. KM was funded by a NERC Studentship; JSG acknowledges receipt of a 2001 Lancaster  
549 University Small Grant; DM received support from the OU Science Staff Tutor research fund; and JAN would  
550 like to thank Sernageomin's PRV and Fondecyt Project No. 1960186.  
551

#### 552 **References**

553  
554 Broecker WS and Denton GH (1990) What drives glacial cycles? *Scientific American* 262:42-50  
555

556 Cas RAF and Wright JV (1987) Volcanic Successions – Modern and Ancient. Allen & Unwin, London  
557

558 Clavero JE, Sparks SJ, Polanco E and Pringle MS (2004) Evolution of Parinacota volcano, Central Andes,  
559 Northern Chile. *Revista Geológica de Chile* 31(2):317-347  
560

561 DeGraff JM, Long PE and Aydin A (1989) Use of joint-growth directions and rock textures to infer thermal  
562 regimes during solidification of basaltic lava flows. *J Volcanol Geotherm Res* 38:309-324  
563

564 Déreulle B and Déreulle J (1974) Los volcanes Cuaternarios de los Nevados de Chillán y reseña sobre el  
565 volcanismo Cuaternario de los Andes Chilenos. *Estudios Geológicos* 30:91-108  
566

567 Dixon HJ, Murphy MD, Sparks RSJ, Chávez R, Naranjo JA, Dunkley PN, Young SR, Gilbert JS and Pringle  
568 MR (1999) The geology of Nevados de Chillán volcano, Chile. *Revista Geológica de Chile* 26(2):227-  
569 253  
570

571 Gilbert JS, Stasiuk MV, Lane SJ, Adam CR, Murphy MD, Sparks RSJ and Naranjo JA (1996) Non-explosive,  
572 constructional evolution of the ice-filled caldera at Volcán Sollipulli, Chile. *Bull Volcanol* 58:67-83  
573

574 Harford CL, Pringle MS, Sparks RSJ and Young SR (2002) The volcanic evolution of Montserrat using  
575  $^{40}\text{Ar}/^{39}\text{Ar}$  geochronology. In: Druitt TH and Kokelaar BP (eds) *The eruption of Soufrière Hills Volcano,*  
576 *Montserrat, from 1995 to 1999.* Geol Soc London Mem 21  
577

578 Lescinsky DT and Fink JH (2000) Lava and ice interaction at stratovolcanoes: Use of characteristic features to  
579 determine past glacial extents and future volcanic hazards. *J Geophys Res* 105(B10):23,711-23,726  
580

581 Lescinsky DT and Sisson TW (1998) Ridge-forming, ice-bounded lava flows at Mount Rainier, Washington.  
582 *Geology* 26(4):351-354  
583

584 Lowe JJ and Walker MJC (1997) *Reconstructing Quaternary Environments* (2nd Edition), Pearson Prentice  
585 Hall, England  
586

587 Lowell TV, Heusser CJ, Andersen BG, Moreno PI, Hauser A, Heusser LE, Schlichter C, Marchant DR and  
588 Denton GH (1995) Interhemispheric Correlation of Late Pleistocene Glacial Events. *Science*  
589 269(5230):1541-1549  
590

591 Mee K, Tuffen H and Gilbert JS (2006) Snow-contact volcanic facies and their use in determining past eruptive  
592 environments at Nevados de Chillán volcano, Chile. *Bull Volcanol* 68:363-376  
593

594 Naranjo JA and Lara LE (2004) August-September 2003 small vulcanian eruption at the Nevados de Chillán  
595 Volcanic Complex (36°50'S), Southern Andes, Chile. *Revista Geologica de Chile* 31(2):359-366  
596

597 Naranjo JA, Chávez R, Sparks RSJ, Gilbert JS and Dunkley P (1994) Nuevos antecedentes sobre la evolución  
598 cuaternaria del complejo volcánico Nevados de Chillán. *Congreso Geológico Chileno 7, Concepción,*  
599 *Chile, 1994* 1:342-345  
600

601 Naranjo JA, Sparks RSJ, Stasiuk MV, Moreno H and Ablay GJ (1992) Morphological, structural and textural  
602 variations in the 1988 - 1990 andesite lava of Lonquimay Volcano, Chile (38°S). *Geol Magazine*  
603 129:657-678  
604

605 Pringle MS (1993) Age progressive volcanism in the Musicians Seamounts: A test of the Hot Spot Hypothesis  
606 for the Late Cretaceous Pacific. In: Pringle MS, Sager WW, Sliter VW and Stein S (eds) *The Mesozoic*  
607 *Pacific: Geology, Tectonics and Volcanism. AGU Geophysical Monograph Series* 77:187-215  
608

609 Singer BS and Pringle MS (1996) Age and duration of the Matuyama-Brunhes geomagnetic polarity reversal  
610 from  $^{40}\text{Ar}/^{39}\text{Ar}$  incremental heating analyses of lavas. *Earth Planet Sci Lett* 139:47-61  
611

612 Singer BS, Jicha BR, Harper MA, Naranjo JA, Lara LE and Moreno-Roa H (2008) Eruptive history,  
613 geochronology and magmatic evolution of the Puyehue-Cordon Caulle volcanic complex, Chile. *Geol*  
614 *Soc Am Bull* 120(5-6):599-618  
615

616 Sumner JM and Branney MJ (2002) The emplacement history of a remarkable heterogeneous, chemically  
617 zoned, rheomorphic and locally lava-like ignimbrite: 'TL' on Gran Canaria. *J Volcanol Geotherm Res*  
618 115(1-2):109-138  
619  
620 Taylor JR (1982) *An introduction to error analysis*. University Science Books, Mill Valley, California  
621  
622 Thouret JC, Cantagrel J-M, Robin C, Murcia A, Salinas R and Cepeda H (1995) Quaternary eruptive history  
623 and hazard-zone model at Nevado del Tolima and Cerro Machin volcanoes, Colombia. *J Volcanol*  
624 *Geotherm Res* 66(1-4):397-426  
625  
626 Tuffen H, Gilbert JS and McGarvie DW (2001) Products of an effusive subglacial eruption: Bláhnúkur,  
627 Torfajökull, Iceland. *Bull Volcanol* 63:179-190  
628  
629 Tuffen H, McGarvie DW, Gilbert JS and Pinkerton H (2002a) Physical volcanology of a subglacial-to-  
630 emergent rhyolitic tuya at Rauðufossafjöll, Torfajökull, Iceland. In: Smellie JL and Chapman MG (eds)  
631 *Volcano-ice interaction on Earth and Mars*. *Geol Soc London Spec Pub* 202:213-236  
632  
633 Tuffen H, Pinkerton H, McGarvie DW and Gilbert JS (2002b) Melting of a glacier base during a small-volume  
634 subglacial rhyolite eruption: evidence from Bláhnúkur, Iceland. *Sediment Geol* 149:183-198  
635  
636 York D (1969) Least squares fitting of a straight line with correlated errors. *Ear Planet Sci Lett* 5:320-324

## Figure/Table Captions (Parentheses indicates approximate placement of Tables and Figures)

### Table 1 (Line 77)

Summary of field observations for newly mapped units at Cerro Blanco.

### Table 2 (Line 77, below Table 1)

Selected representative geochemical and petrologic analyses of newly mapped units at Cerro Blanco .

### Table 3 (Line 264)

Summary of new and existing  $^{40}\text{Ar}/^{39}\text{Ar}$  analyses from Cerro Blanco.

### Figure 1 (Line 36)

Location map of the northwestern region of Nevados de Chillán Volcanic Complex, showing the locations around the Cerro Blanco subcomplex referred to throughout this paper. Base map: Nevados de Chillán Sheet 3645-7115, Instituto Geográfico Militar de Chile. Inset shows location of Nevados de Chillán within Chile.

### Figure 2 (Line 45)

Nevados de Chillán Volcanic Complex, with the Cerro Blanco subcomplex (NW) at left and Las Termas subcomplex (SE) at right (viewed looking east). The two subcomplexes are approximately 6 km apart.

### Figure 3 (Line 62)

Geologic map of the Cerro Blanco subcomplex.

### Figure 4 (Line 107)

Schematic diagram showing the southern cliffs of the Upper Santa Gertrudis valley.

### Figure 5 (Line 119)

The inter-bedded lava and scoria layers that comprise the outer caldera wall cliffs (OC1); viewed from the North Ridge and looking N.

### Figure 6 (Line 130)

Southern section of the inner caldera wall, showing the distribution of the newly mapped IC1, IC2 and IC3 units. The view is looking SW from the top of the North Ridge and the field of view is approximately 1 km wide.

### Figure 7 (Line 140)

Schematic diagram of IC1 inner caldera wall lavas at the southern end of the inner caldera wall. At least six individual lava flows are observed and can be traced laterally for ~ 100 m, although irregularities on the cliff face make it difficult to trace all of the flows along the entire length of the cliff section (~ 500 m). Not to scale.

### Figure 8 ((Line 145)

Relationship between the IC1, IC2 and IC3 units in the volcano-facing scarp at the southern end of the inner caldera wall. The view is looking W, away from the summit of Cerro Blanco and the field of view is approximately 200 m wide. [\*  $\text{Ar}^{40}/\text{Ar}^{39}$  age is from Dixon et al., 1999].

### Figure 9 (Line 166)

Schematic diagram showing the structure of the IC2 vent at the southern end of the inner caldera wall. Inset 1 shows the typical structure of an individual bed and Inset 2 shows the contact between the vent-fill breccia and the underlying andesitic intrusion.

### Figure 10 (Line 178)

Photograph and sketch of the North Ridge at the northern end of the inner caldera wall: (a) showing the dimensions of the North Ridge, with inset showing part of the IC3 subglacial lobes; (b) showing the distribution of different facies on the North Ridge. View is looking S, from the outer caldera wall.

### Figure 11 (Line 200)

The IC3 unit at the southern end of the inner caldera wall: (a) distribution of the subglacial lava lobes on the col region of the inner caldera wall and the sills that breached the ground surface above the col (inset); (b) the two larger subglacial lobes on the col; (c) detailed view of one of the lobes, showing a partial cross-section through

the centre of the lobe; and (d) annotated sketch of the lobe in (c), showing the general structure of the subglacial lobes.

**Figure 12 (Line 387)**

Palaeoenvironment reconstruction showing the approximate level of ice at the time of emplacement of the IC3 sills, dykes and subglacial lobes.

**Figure 13 (Line 492)**

Chronology of volcanic activity at Cerro Blanco compared with oxygen isotope variations over the past 120 ka. Isotopically light values (warmer conditions) to the left and isotopically heavier values (cooler conditions) to the right. Marine oxygen isotope stages (MOIS) are given on the right. The isotopic signal is interpreted as a proxy for extent of global palaeoglaciation. The vertical line represents the isotope ratio that corresponds to the limited ice cover typical of the Holocene. Modified after Broecker and Denton (1990) and Lowe and Walker (1997).

Table 1

Unit	Unit Name / Facies	Geomorphology / Structure	Texture / Fracture Types
SGV1	North Santa Gertrudis Valley (SGV) Lavas	150-200m high cliffs – upper regions comprise: 10-20cm wide columns, <1m length, variable orientation	Reddish-brown, strongly altered, massive lava (NB: Poor accessibility meant only upper parts of cliffs could be seen through binoculars)
SGV2	South Santa Gertrudis Valley (SGV) Lavas	150m high cliffs comprising zones of massive/weathered lava, columnar jointed lava and fine-grained, bedded deposits (see Fig. 4)	Huge complexity in textures and fracture types – detailed observations limited due to access
SGV3	Outer Caldera Wall Lavas	50-100m high cliffs, 2.5km long; 10 lava flow deposits, 5-10m thick, inter-bedded with lens-shaped patches of red oxidised scoria	Smooth/striated upper surfaces at western end; broad vertical joints towards eastern end; holocrystalline, devitrified
	Outer Caldera Wall Breccias	20m v-shaped patch at base of OCW lavas to west of SGV; 50m v-shaped patch on east side of SGV (observations through binoculars only)	No detailed observations due to limited access
IC1	Inner Caldera Wall Lavas	6 lava flow deposits (see Fig. 7), each 3-8m thick, extend laterally 10-100m; dip 5-10° W away from Cerro Blanco summit	Lavas 1, 2, 5 and 6: porphyritic, broad columnar jointing, scoriaceous upper margins. Lavas 3 and 4: some bulbous lobes, glassy/hackly-jointed exterior. Lavas separated by irregular patches of breccia, clasts up to 40cm diameter in fine-grained matrix (Fig. 7)
IC2	Lanahue Vent Facies: <i>Welded breccia and spatter</i>	Multiple beds to south of vent, increasing dip from near horizontal at base to 45° N at top of succession. Beds are 0.25-3m thickness.	See Fig. 9
	Lanahue Vent Facies: <i>Massive andesite body</i>	8m thick, andesite intrusion, exposed at base and to north side of centre of Lanahue Vent	Massive, crystal-rich, highly vesicular: vesicles sub-mm to >45 cm diameter accumulations. Gradational contact between intrusion and breccia (see Fig. 9)
	North Ridge Vent Facies: <i>North Ridge Lavas</i>	Several lava flow deposits, form bedded semi-circle at southern end of North Ridge (2400m elevation); lava strongly eroded/polished with 2 sets of striae to N	Lavas have red scoriaceous tops, platy centre; to north (2350m elevation), lava shows greater degree of welding and no scoriaceous top
	North Ridge Vent Facies: <i>Upper Santa Gertrudis Valley (USGV) lavas</i> (See Mee et al., 2006)	3 geomorphologic zones: Zone 1 (2300-2260m elevation) elongate lobes 8-13m long, 4-6m wide, 2-3m high; Zone 2 (2250m) Several interconnected bulbous lobes on plateau; Zone 3 (2250-220m) Steep-sided lava	<i>Zone 1:</i> Autobreccia and pseudopillow fractures; <i>Zone 2:</i> Glassy outer carapace, crystalline interiors, hyaloclastite around base; <i>Zone 3:</i> Glassy outer carapace, narrow columnar joints orthogonal to outer surface and hyaloclastite

Table 2

<b>Unit Name</b>	<b>SGV1</b>	<b>OC1</b>	<b>(IC1) Lanalhue Caldera Wall Lavas</b>						<b>(IC2) ICW Vent Facies</b>			<b>(IC3) Glassy Lava Lobes</b>	
<b>Facies and Sub-facies Names</b>	<b>North SGV lavas</b>	<b>Outer Caldera Wall Lavas</b>	<b>Lava 1</b>	<b>Lava 2</b>	<b>Lava 3</b>	<b>Lava 4</b>	<b>Lava 5</b>	<b>Lava 6</b>	<b>Welded breccia/spatter</b>	<b>Vesicular Intrusion</b>	<b>USGV Lava</b>	<b>Lava Lobes</b>	<b>Platy sills/dykes</b>
<b>Sample No.</b>	<b>CB53</b>	<b>CB59</b>	<b>CB23</b>	<b>CB24</b>	<b>CB48</b>	<b>CB26</b>	<b>CB27</b>	<b>CB30</b>	<b>CB35</b>	<b>CB74</b>	<b>CB55</b>	<b>CB02</b>	<b>CB43</b>
<b>SiO<sub>2</sub></b>	60.96	60.17	55.15	54.07	59.12	58.17	62.94	65.33	59.03	58.92	58.37	57.52	60.58
<b>TiO<sub>2</sub></b>	1.36	1.64	1.00	0.99	1.09	1.25	0.94	0.92	1.39	1.42	1.07	1.28	1.44
<b>Al<sub>2</sub>O<sub>3</sub></b>	16.33	15.20	18.01	17.57	17.34	16.17	16.33	15.71	16.53	16.02	17.11	17.00	16.85
<b>Fe<sub>2</sub>O<sub>3</sub></b>	7.13	8.00	8.22	8.21	6.61	7.63	5.97	5.23	7.21	8.02	7.15	7.92	6.72
<b>MnO</b>	0.13	0.14	0.13	0.14	0.12	0.13	0.10	0.09	0.14	0.14	0.11	0.14	0.13
<b>MgO</b>	2.09	2.40	4.42	4.93	3.06	3.42	2.27	1.70	2.26	2.62	3.32	3.24	1.93
<b>CaO</b>	4.66	4.85	8.66	8.65	5.96	6.66	4.76	3.81	4.37	5.70	6.67	6.75	4.12
<b>Na<sub>2</sub>O</b>	5.00	4.74	3.86	3.71	4.55	4.06	4.45	4.48	5.58	4.71	4.19	4.36	5.54
<b>K<sub>2</sub>O</b>	2.15	1.75	0.68	0.71	1.78	1.42	1.91	2.35	1.95	1.44	1.43	1.17	1.94
<b>P<sub>2</sub>O<sub>5</sub></b>	0.35	0.54	0.19	0.19	0.23	0.27	0.20	0.20	0.43	0.36	0.25	0.39	0.47
<b>SO<sub>3</sub></b>	0.01	0.00	0.00	0.00	0.00	0.01	0.00	0.00	0.01	0.00	0.00	0.00	0.01
<b>Rb</b>	64.50	36.70	68.91	96.84	54.38	41.13	45.49	67.17	54.68	68.11	50.26	42.33	54.50
<b>Sr</b>	395.2	535.3	360.02	333.63	451.09	509.68	476.24	378.69	395.77	385.40	433.82	471.25	388.70
<b>Y</b>	30.5	18.9	35.78	40.31	22.68	26.34	30.45	32.61	38.51	31.50	30.57	27.64	35.90
<b>Zr</b>	242.7	129.7	270.08	299.61	182.75	169.82	189.02	246.59	221.61	246.81	215.86	169.61	239.20
<b>Rock Type</b>	A	A	BA	BA	A	A	A	D	A	A	A	B-A	A
<b>Phenocrysts %</b>	7	10	5-10	5-10	5-10	5-10	5-10	5-10	<5	n/a	<5	5	15
<b>Phenocryst assemblage</b>	f + cpx + opx + ores + ap	f + cpx + opx + ol + ores	f + cpx + opx + ol + ores	f + cpx + opx + ol + ores	f + cpx + opx + ores	f + cpx + opx + amp + ores + ap	f + cpx + opx + ores + ap	f + cpx + opx + ores + qtz + ap	f + cpx + opx + ores	f + cpx + opx + ol + ores	f + cpx + opx + ol + ores	f + cpx + opx + ol + ores	f + cpx + opx + cpx + ores

Key: A = Andesite; BA = Basaltic-andesite; f = feldspar; cpx = clinopyroxene; opx = orthopyroxene; ol = olivine; amp = amphibole; ap = apatite; qtz = quartz; ores = Fe-Ti oxides

All samples from Nevados de Chillán collected for this project between 02/2001 and 04/2002 and analysed at the XRF Facility at the University Leicester.

Samples were numbered in order of collection and prefixed "CB" for Cerro Blanco.

Table 3

New <sup>40</sup> Ar/ <sup>39</sup> Ar Analyses												
Sample No.	Unit	Sample Type	Total Gas Age		No. of steps*	Age Spectrum				Isochron Analysis		
			K/Ca	Age ± 2 s.d. (ka)		Furnace Power	<sup>39</sup> Ar (%)	Age ± 2 s.d. (ka)	MSWD #	Age ± 2 s.d. (ka)	MSWD #	<sup>40</sup> Ar/ <sup>36</sup> Ar Intercept
CB14 <sup>1</sup>	IC3	wr core	0.546	75.6 ± 0.7	7 of 15	8.0 to 11.0	71.8	80.0 ± 0.6	1.75	80.9 ± 1.4	2.06	291.7 ± 4.7
CB14 <sup>2</sup>	IC3	wr core	0.538	73.9 ± 1.0	8 of 14	7.0 to 12.0	91.3	79.9 ± 0.6	1.20	79.6 ± 1.2	1.35	297.2 ± 4.2
CB74	IC2	gr mass	0.533	103.0 ± 3.5	8 of 17	6.6 to 8.7	62.4	92.4 ± 3.5	2.38	95.6 ± 16.6	3.86	294.5 ± 4.5
CB55	IC2	wr core	0.322	76.3 ± 2.3	7 of 16	8.0 to 10.5	55.8	90.0 ± 0.6	0.57	90.7 ± 1.2	0.54	293.7 ± 2.5
CB83	IC2	wr core	0.327	87.0 ± 1.5	10 of 14	6.2 to 13.5	83.0	88.9 ± 1.0	1.04	88.5 ± 1.5	1.17	295.6 ± 0.9

Published <sup>40</sup> Ar/ <sup>39</sup> Ar Analyses (Dixon et al., 1999)												
Sample No.	Unit	Sample Type	Total Gas Age		No. of steps*	Age Spectrum				Isochron Analysis		
			K/Ca	Age ± 2 s.d. (ka)		Increments used (°C)	<sup>39</sup> Ar (%)	Age ± 2 s.d. (ka)	MSWD #	Age ± 2 s.d. (ka)	MSWD #	<sup>40</sup> Ar/ <sup>36</sup> Ar Intercept
C-9	CB2b	wr core	0.940	19.0 ± 2.6	10 of 12	600-1150	86.5	14.9 ± 0.9	0.78	14.2 ± 1.1	0.71	296.5 ± 1.3
C-27	CB2a	wr core	0.312	53.1 ± 5.1	7 of 11	525-1350	86.8	26.2 ± 2.5	0.73	23.9 ± 2.7	0.74	296.8 ± 0.8
C-90	CB1 <sup>3</sup>	wr core	0.614	93.3 ± 1.7	4 of 9	825-1100	53.8	82.9 ± 1.8	0.37	81.5 ± 4	0.56	296.8 ± 3.2
97-01	LP	wr core	0.279	803.3 ± 18	6 of 11	700-1100	45.0	640 ± 14	5.3	641 ± 20	4.3	295 ± 1.5

\* Number of increments used in regression

# F Variate Critical Value i.e. the MSWD value should be less than this number for the age to be accurate at the 99% confidence level

Analytical methods and data reduction are summarised in Singer and Pringle (1996)

All ages relative to 28.34 Ma for Taylor Creek Rhyolite sanidine TCR-2a (85G0033)

<sup>1</sup> First split of sample

<sup>2</sup> Second split of sample

<sup>3</sup> Field mapping during this study has confirmed this sample to be from the IC3 unit)

<sup>4</sup> Low-precision results from subglacial lavas, generally caused by large 'trapped-gas' components - included primarily for completeness

Figure 1

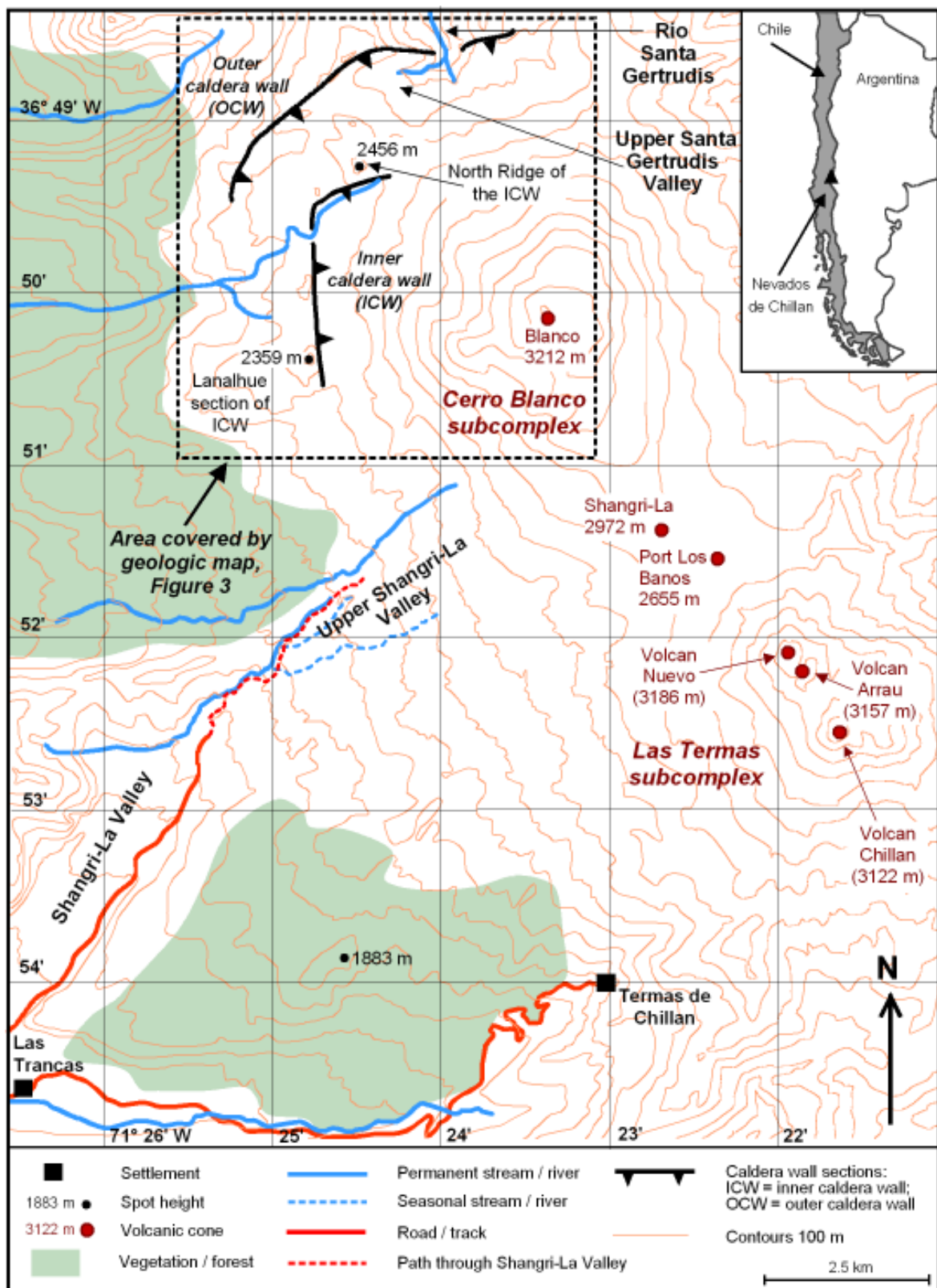


Figure 2



Figure 3

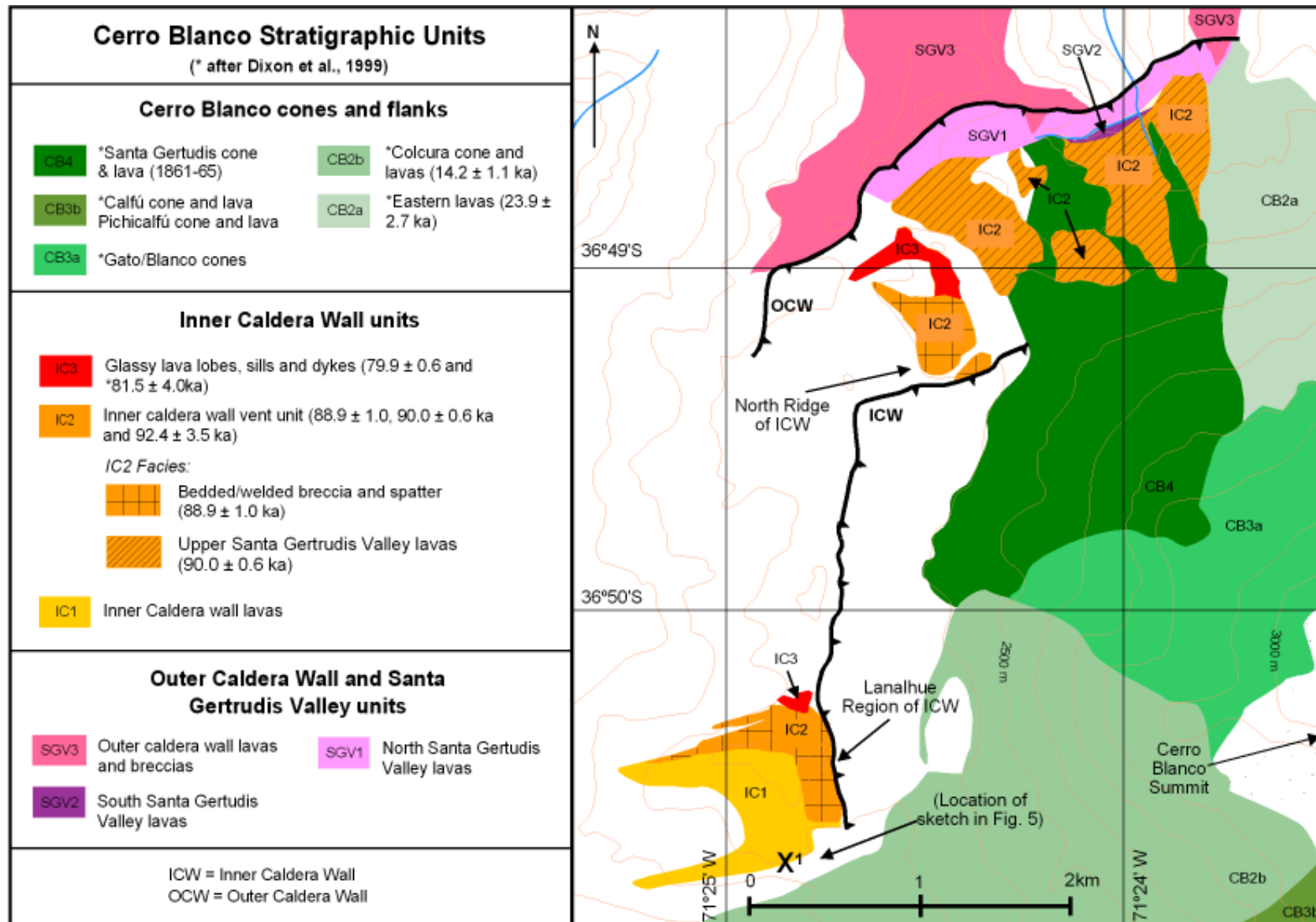


Figure 4

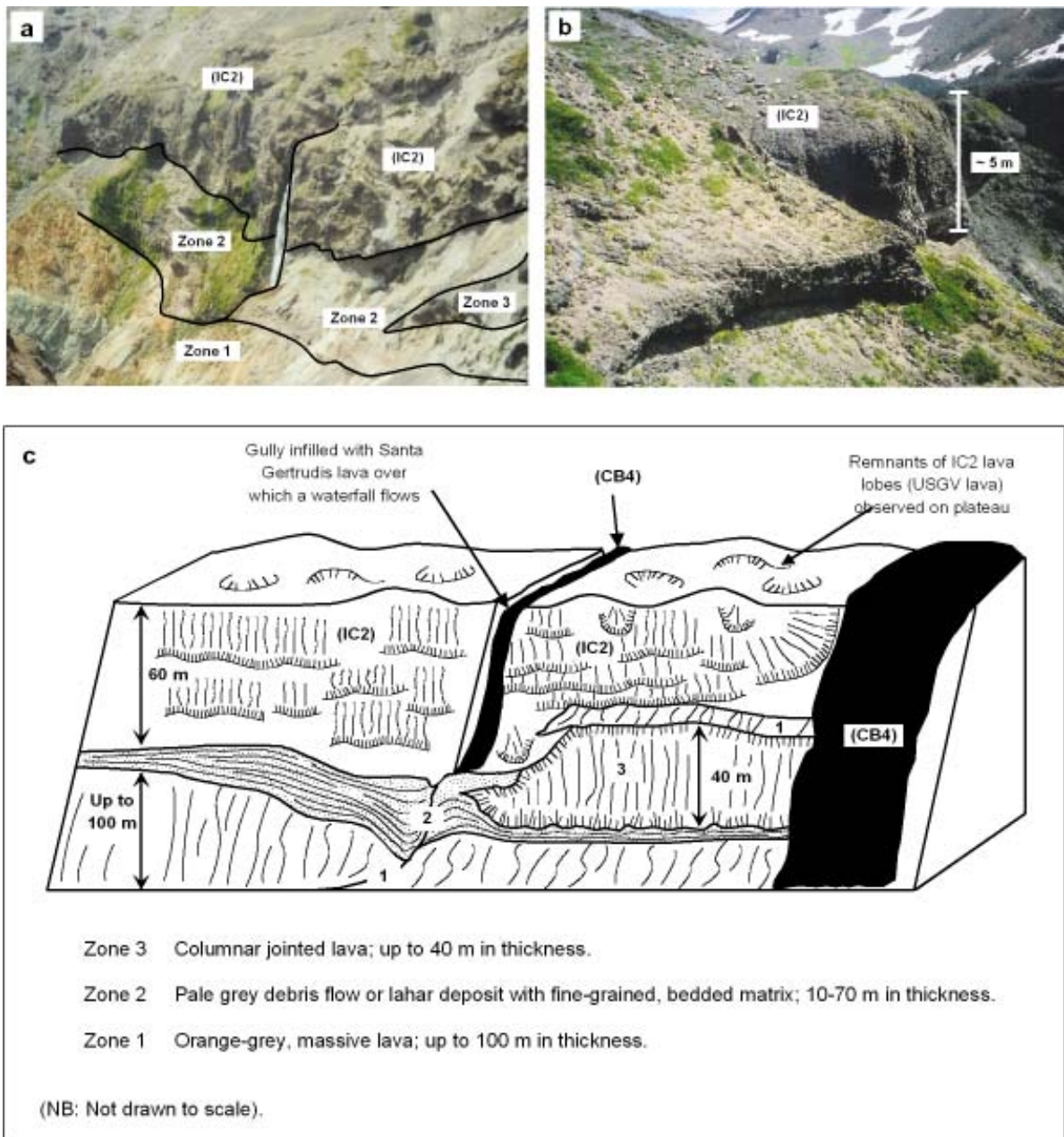


Figure 5

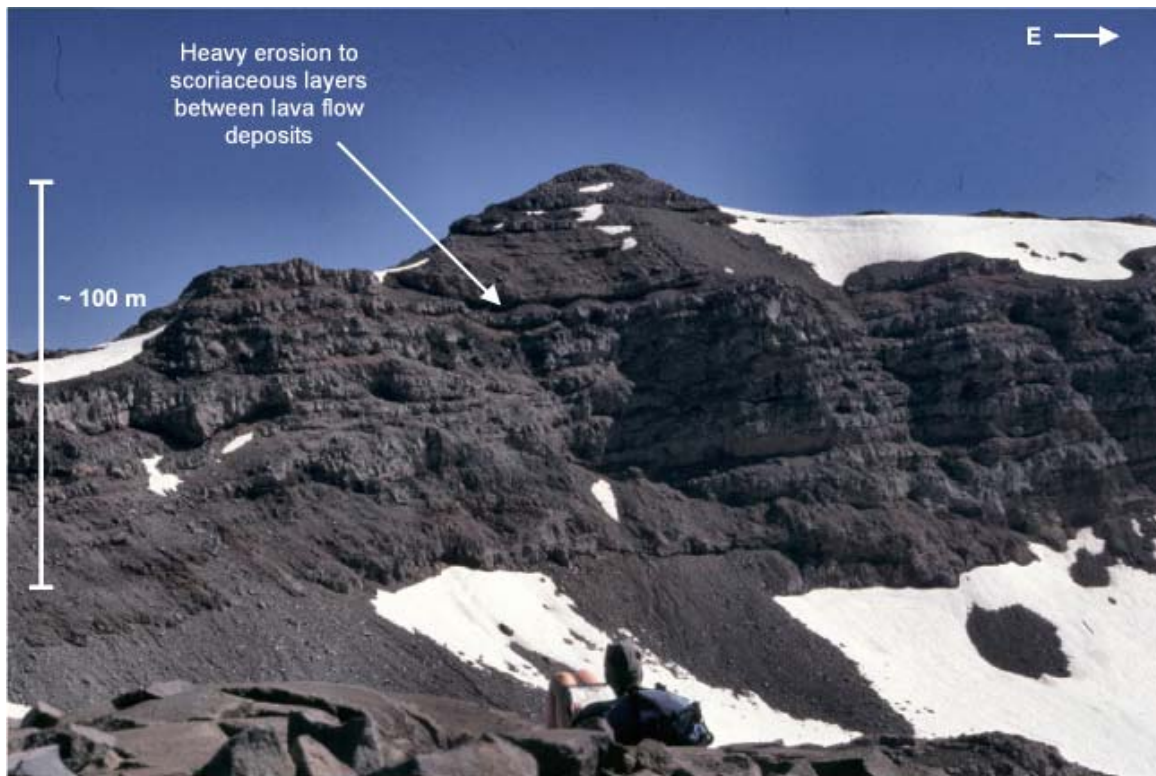


Figure 6

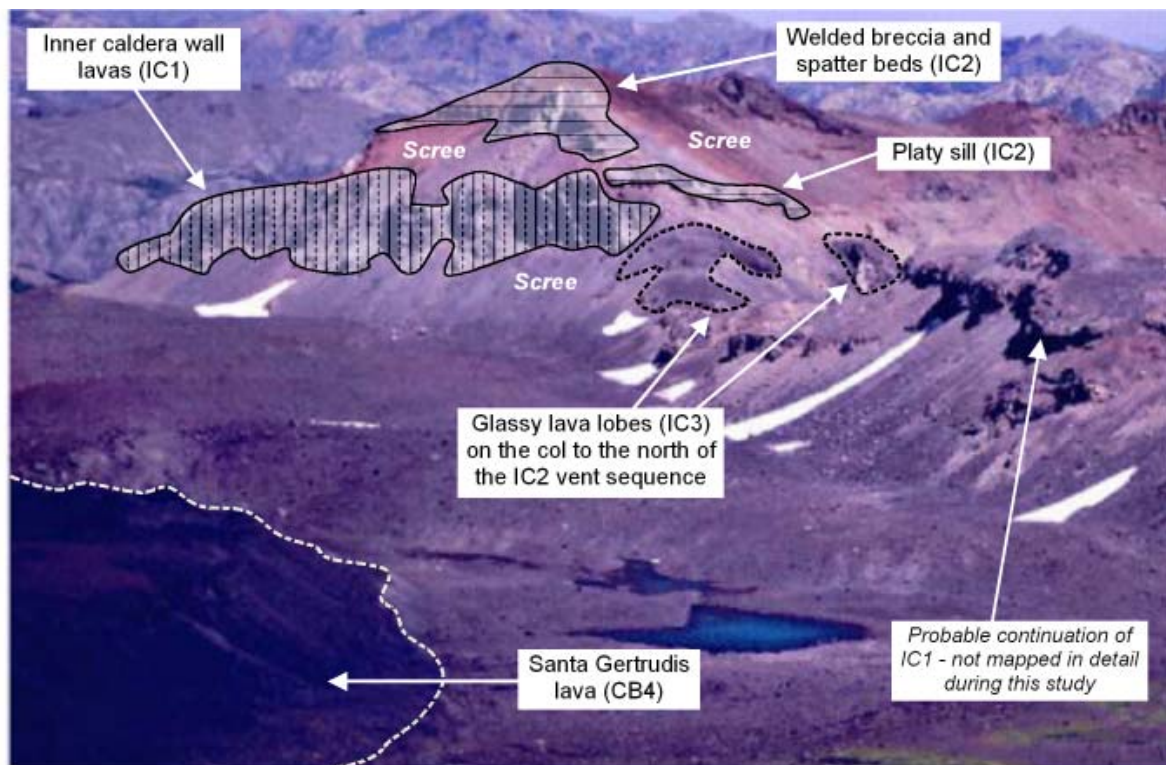


Figure 7

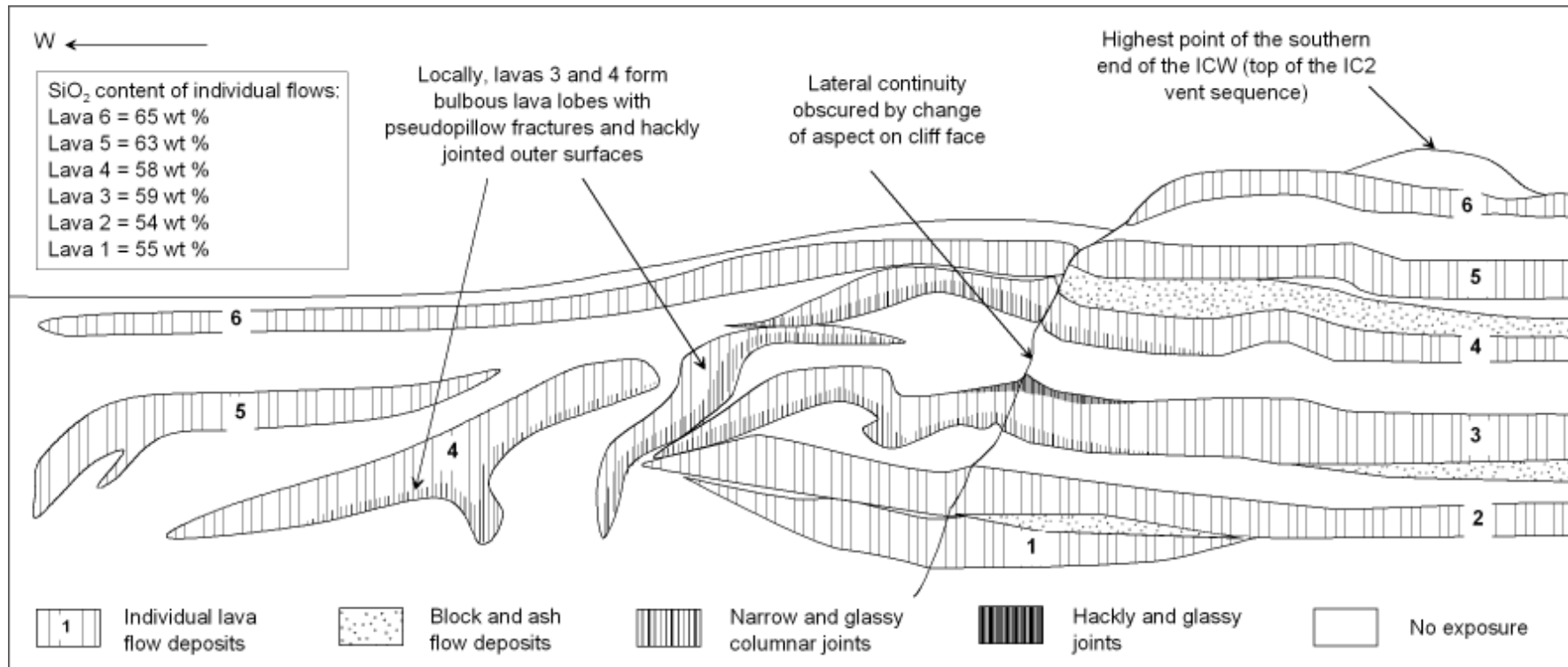


Figure 8

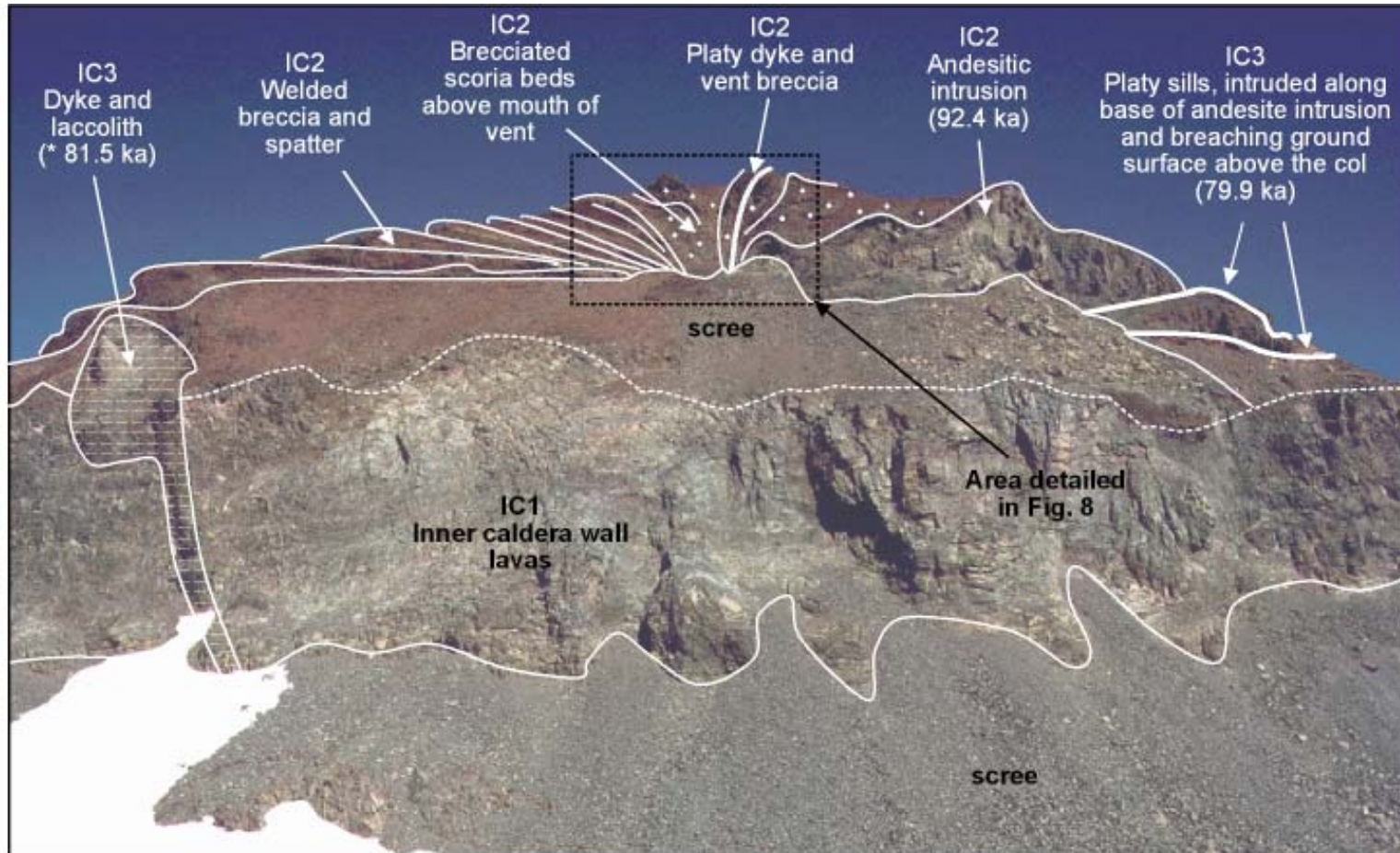


Figure 9

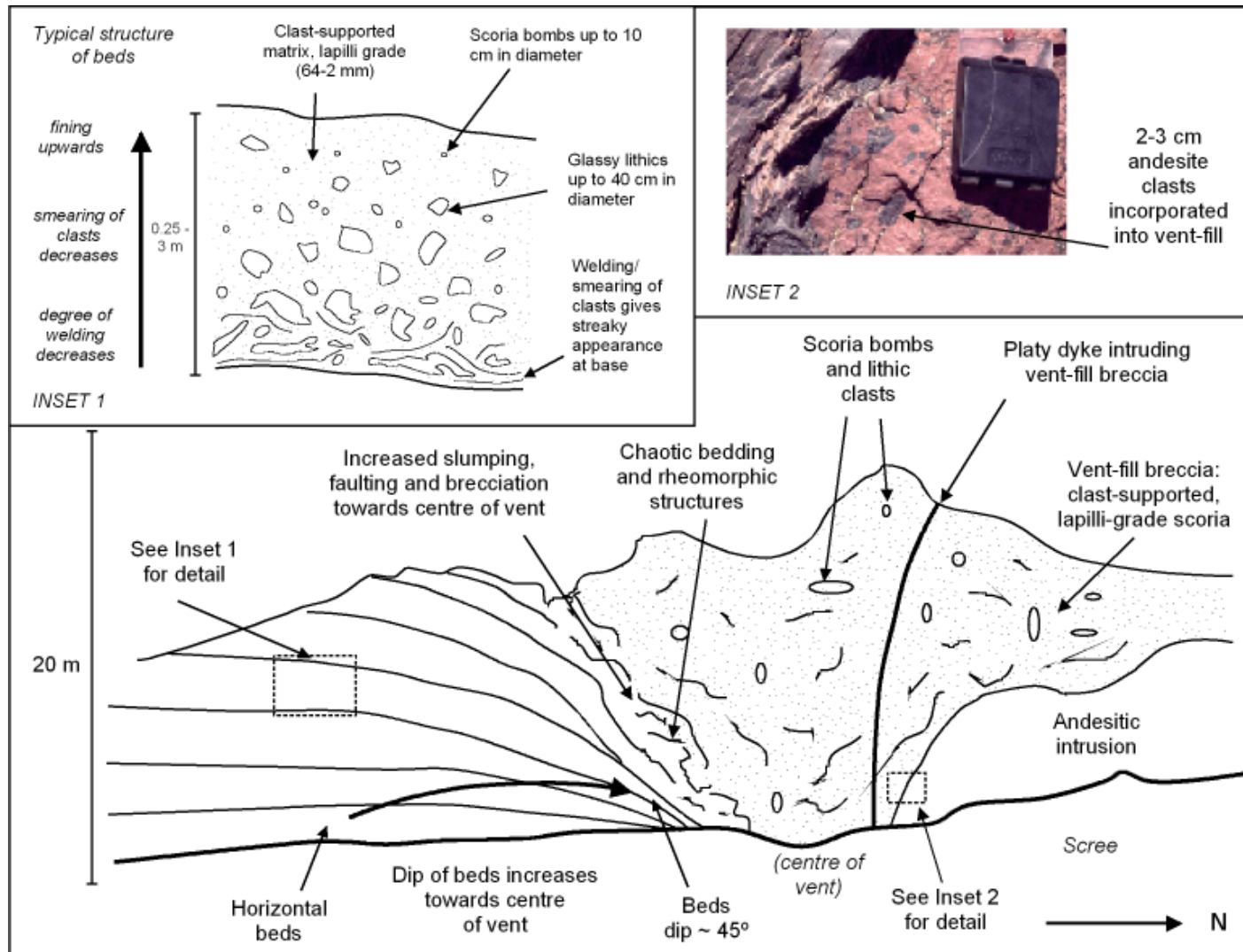


Figure 10

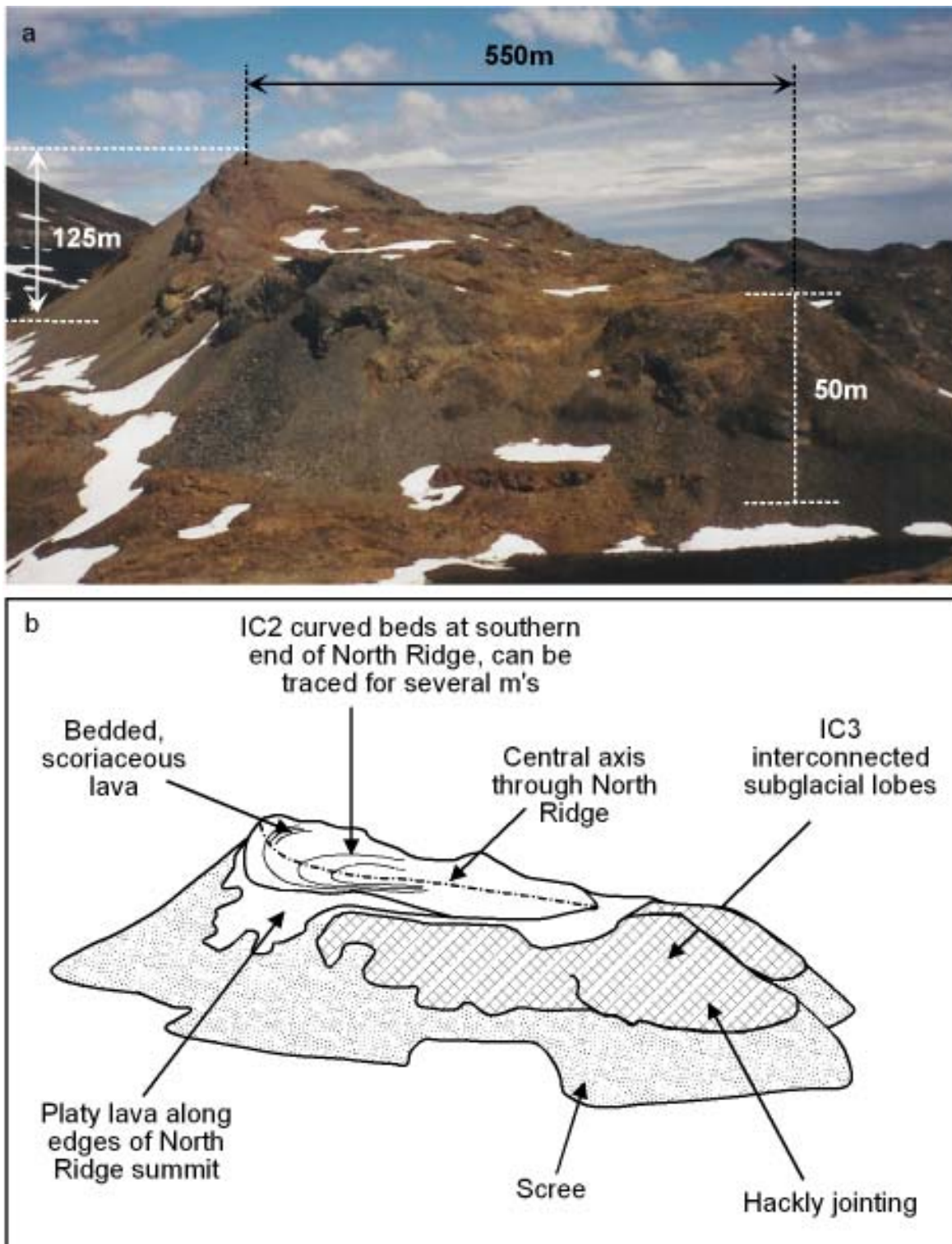


Figure 11

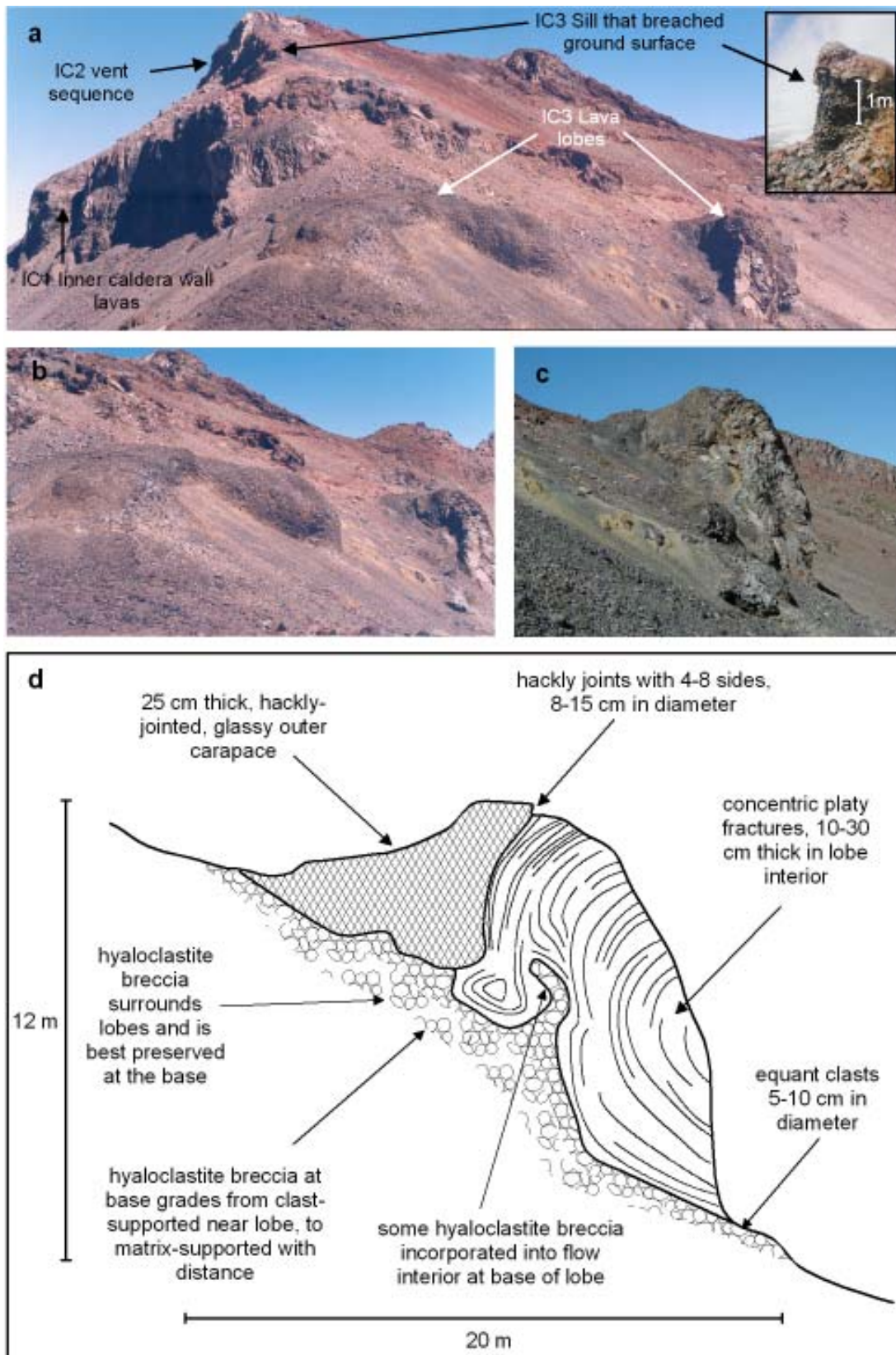


Figure 12

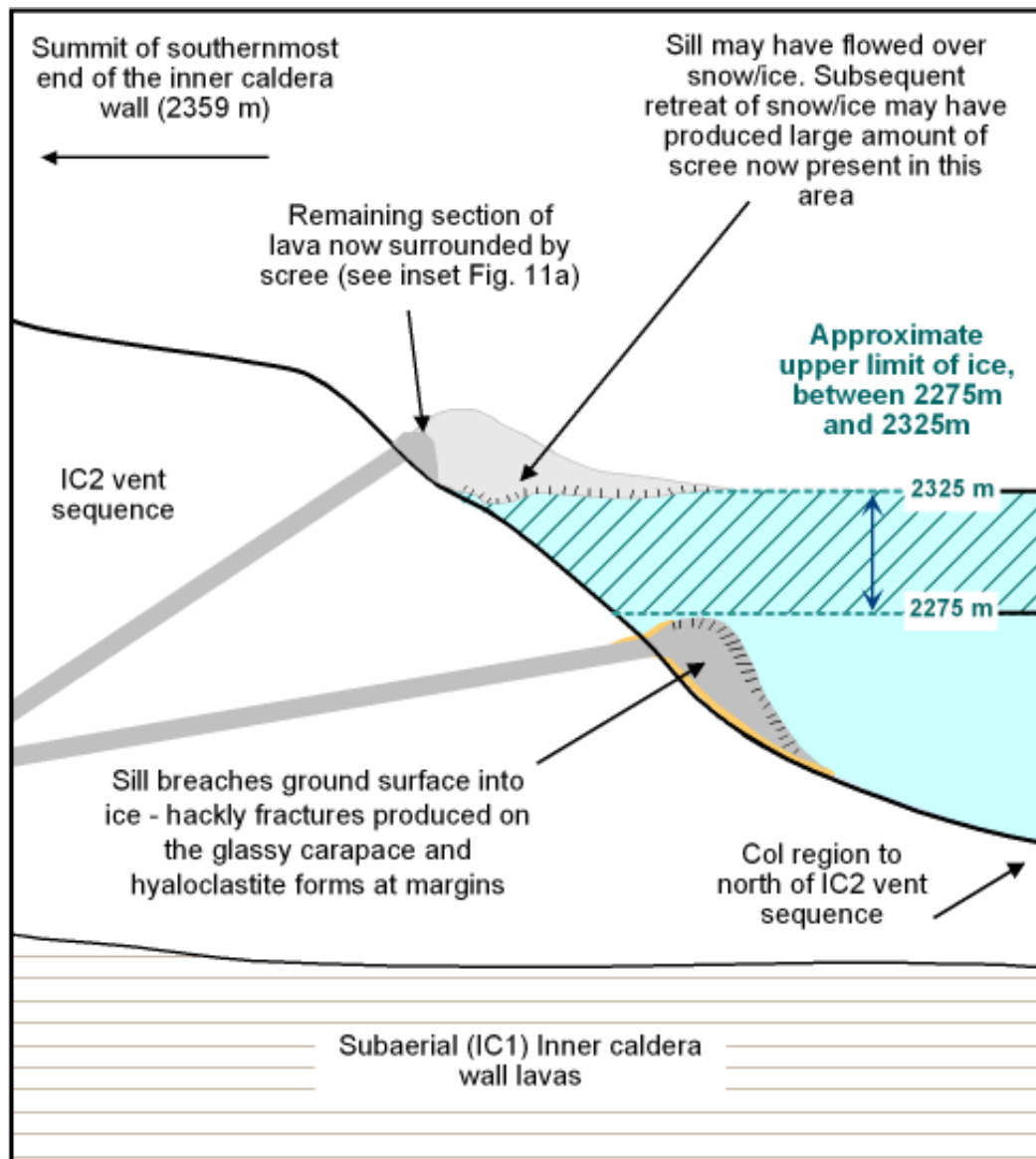


Figure 13

